DEPARTMENT OF BIOLOGICAL AND ECOLOGICAL SCIENCES (DEB)

XXVI PhD course in Genetics and Cellular Biology

BIO/11

Analysis of Tap73-dependet signaling via integrated Omics technologies

Coordinator:

Prof. Giorgio Prantera

Tutor:

Prof. Lello Zolla

PhD student:

Dott.ssa Cristina Marrocco

Index

Aim of the study

In 1997, p73 emerged as a structural and functional homolog of the tumor suppressor p53 [1]. p73 and p53 genes consist of an N-terminal transactivation domain, a central sequence-specific DNA-binding domain, and a C-terminal oligomerization domain respectively [2, 3]. The human p73 genes are composed of 15 exons spanning over 80 000 bp on chromosome 1p36.3 [2]. Contrary to p53, p73 gene is very complex, since it expresses at least seven alternatively spliced C-terminal isoforms (α, β, γ, δ, ε, ζ and η – also referred to as transactivation proficient or TA variants) and at least four alternatively spliced N-terminal isoforms initiated at different ATG (including ΔNp73α and ΔNp73β, lacking the transactivation domain) [2-5]. Alternatively spliced TA isoforms display different transcriptional and biological properties. Based on their sequence similarity at the DNA binding domain, it is not surprising that p53 and TAp73 isoforms can share some transcriptional targets and, as a consequence, elicit similar biological effects. Ectopic expression of TAp73 isoform is indeed able to transactivate p53-responsive genes causing cell cycle arrest and apoptosis [2]. TAp73-triggered apoptosis follows several pathways [6-8], including mitochondrial intrinsic pathway (through activation of PUMA [9], Noxa [10] and Bax [6]) and via endoplasmic reticulum (ER) stress through the induction of Scotin [11]. Pro-apopotic activity of TAp73 variants can be modulated [12,13] by phosphorylation of TAp73 via checkpoint kinase Chk1 and Chk2 [14] or AMPK [15], or through collaborative binding to c-Abl [16,17].

In contrast to the TAp73 isoforms, the ΔN variants ΔNp73α and ΔNp73β, which are generated by alternative promoter utilization, exhibit dominant-negative behavior toward wild-type p73 as well as p53, display anti-apoptotic and oncogenic activity and it is involved in the regulation of the DNA damage checkpoint response [18-22]. Thus, the pro-apoptotic activity of p73 is determined by the relative expression levels of its TAp73 and dominant-negative ΔNp73 variants in cells [23]. However, exceptions to this assumption are all but infrequent, especially in the light of recent reports indicating a controversial role of the TAp73α isoform in mitigating apoptotic events in K-562 leukemia cells [24], small cell lung carcinoma [25,26], and human ovarian carcinoma cell line A2780 [27]. Therefore, although TAp73 isoforms are able to bind specifically to DNA through p53 responsive elements, transcriptional targets of p73 isoforms and p53 can not be entirely comparable, and thus their biological functions. Accordingly, the analysis of the isoform specific p73 knock-out mice revelead a peculiar function of p73 during

neurodevelopment, mitotic spindle checkpoint and DNA damage checkpoint response, suggesting that p73 biological functions are not entirely redundant with those of p53.

Besides activating the transcription of genes-encoding proteins, p73 is also able to upregulate the expression of miRNAs, such as let-7, miR-34, miR-15/16a, miR-145, miR-29, miR-26, miR-30, miR-146a [28] and miR-200 family [29]. While connections between miRNAs and cancer cell metabolism are increasingly being confirmed [30,31], the actual effect of TAp73 expression in cancer cell metabolism still remain under-investigated. Indeed, energy metabolism is a key hallmark of cancer [32, 33], and tumor suppressor genes such as p53 play a central role in the modulation of glucose metabolism [34]. So far, available results suggest a role for TAp73α in the dysregulation of mitochondrial energy metabolism and exacerbation of mitochondria-induced ROS production in HCT116 and TAp73 knock out MEF cells [35]. The underlying mechanisms could involve the complex IV subunit cytochrome C oxidase subunit 4 (Cox4i1), a direct target of TAp73α [35].

The aim of this study is to seek a further understanding of the TAp73α-mediated cellular signaling. For this, we performed an integrated omics approach, based upon the simultaneous application of metabolomics, lipidomics, proteomics and phosphoproteomics. The application of multiple omics analyses to the same biological matrix holds several advantages, in that it helps coping with the intrinsic limitations of each independent approach [36], while providing further clues to the understanding of the biological phenomenon under investigation, even when scarce direct overlap among results from different omics is observed [37]. In this view, integration of omics disciplines represents the inevitable evolution of unsupervised approaches, towards the achievement of actual Systems Biology-wide comprehension of living systems [38].

1 INTRODUCTION

1.1 P53 family

The p53 protein family consists of three transcription factors: p53, p63, and p73. P53 was described for the first time in 1979 as a nuclear protein engaged by the oncogenic SV40 large T antigen, and it is the most studied proteins in the cancer field[39]. 18 years after discovery of p53, two p53-related genes were identified: p63 and p73.

Interestingly, p63 and p73 are structurally similar and functionally related to p53, and hence the entire p53 family may be regarded as a unique signaling network controlling cell proliferation, differentiation, and death. The discovery of these p53-related proteins, improve the level of complexity within this family, owing to their simultaneous, exclusive or consecutive physical interactions and ability to act as transcriptional regulators.

These genes encode a lot of protein isoforms through multiple mechanisms including extensive alternative mRNA splicing. According to recent study, approximately 92–95% of human multi-exon genes undergo AS, increasing the amount of functionally different protein isoforms. [40,41]

Phylogenetic analysis of p53 family proves their origin from a p63/73-like ancestral gene early in metazoan evolution. Probably, maintenance of genetic stability of germ cells seems to be its ancestral function. The p53 family regulates many biological processes, including proliferation, cell differentiation, cell death and apoptosis. Abnormal alterations of splicing or dysregulation of the p53 family may interfere with normal cellular homeostasis and lead to cancer development.[54]

1.2 Protein Structure p53 Family

The members of p53 family share a very high structural similarity in protein organization. In fact, they are characterized by similar structure that identify p53 across all species:

- an acidic N-terminal transactivation domain (TAD)
- core DNA-binding domain (DBD)
- and carboxy-terminal oligomerization domain (OD)

Between DBD and OD there is a small nuclear localization signal, responsible for localization in the nucleus (NLS), and at least one proline rich domain (PRD) with PXXP motif (P = proline, and X = any other amino acid) between TAD and OD [47]. Only p63 and p73 have a carboxy-terminal inhibitory region, post SAM domain (PS), and an area with a sterile a-motif (SAM). **(figure.1 a)**

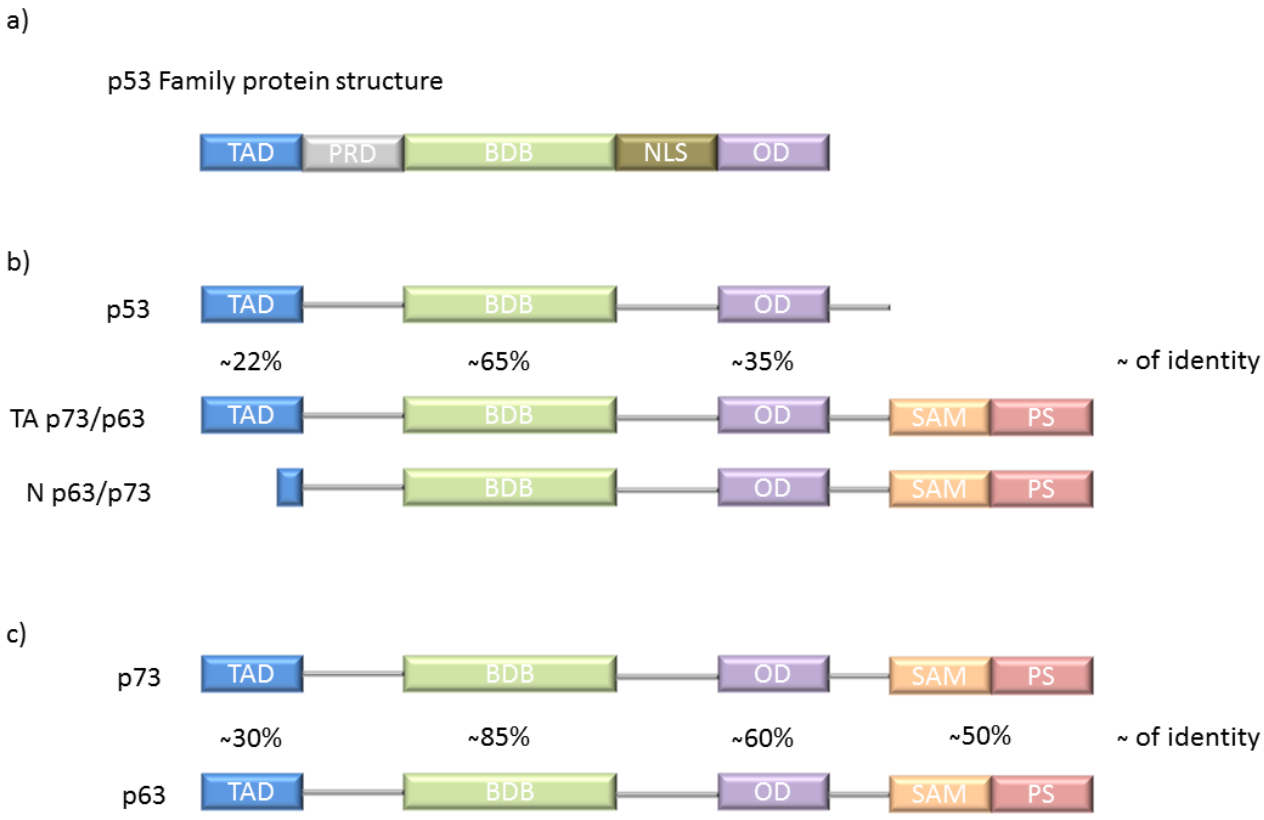

Figure.1 Schematic representation of the protein modular structure of the p53 family members: b)The overall domain structure of p53, p73, and p63 is conserved and consists of an amino-terminal transactivation domain (TAD), a central DNA binding domain (DBD) and a carboxy-terminal oligomerization domain (OD), c) degree of identity between p53, p73 and p63. b) degree of identity between p73 and p63. They are both more homologous to each other than to p53.

The three major domains are highly conserved between the family members.**(figure 1 b)** The transactivation domain (TAD) is the least conserved with ~25% identity between p53 and p63/p73. The core DNA binding domain (DBD) and of p73/p63 are ~ 65% identical with p53.

The C-terminal oligomerization domain (OD) of p53 is 35% identical with p63 and p73. In addition, the residues of p53 that directly interact with DNA are identical in p63 and p73. Consequently, both p63 and p73 can form oligomers, bind DNA, transactivate p53-responsive genes, and mediate cell cycle arrest, thus inducing cell cycle arrest, apoptosis and cellular senescence.

Sequence identity between p73 and p63 is more than to p53. **(figure 1 c)** Analysis of primary amino acid sequence reveal a high degree of identity. In fact, the transactivation domain (TAD) and the DNA binding domain (DBD) of p73 are ~40% and ~85% identical with p63 respectively, the carboxy-terminal oligomerization domain (OD) of p73 is 65% identical with p63 and the area containing sterile a-motif (SAM) and Post-SAM domain of p73 is ~50% identical with p63. Therefore, they are both more homologous to each other than to p53.

Because of splicing events occurring at the carboxy-terminal region and to the presence of an alternative promoter located in the third intron, p53 family members exist as multiple protein variant.

1.3 Genomic Organization of p53 Family

The genomic organization of the p53 family is highly conserved among different species. The human p53 gene is composed approximately of 19 200 bp spanning over 11 exons on chromosome 17p13.1. **(figure 2 a)**

Due to alternative promoter usage and alternative splicing, p53 gene encodes respectively full-length p53 (p53), Δ40p53 and Δ133p53[48]. **(figure 2 b)**

The Δ40p53 (or ΔNp53) can be generated either by alternative initiation of translation or by an alternative splicing on the intron 2 to produce an amino-terminally truncated p53 isoform deleted of the first 40 amino-acid. The full length p53, encoded by the first promotor (P1), is full efficient in transcriptional activity, whilst the variant Δ40p53 protein still contains part of the p53 transactivation domain and can activate gene expression after transfection through a second transactivation domain located between amino-acid 43 and 63. Δ40p53 can also act after transfection, in a dominant-negative manner towards WTp53 inhibiting both p53 transcriptional activity and p53-mediated apoptosis.

The alternative promoter (P2) leads to the expression of an amino-terminally truncated p53 protein initiated at codon 133 (Δ 133p53). Alternative splicing of intron 9 give rise to three

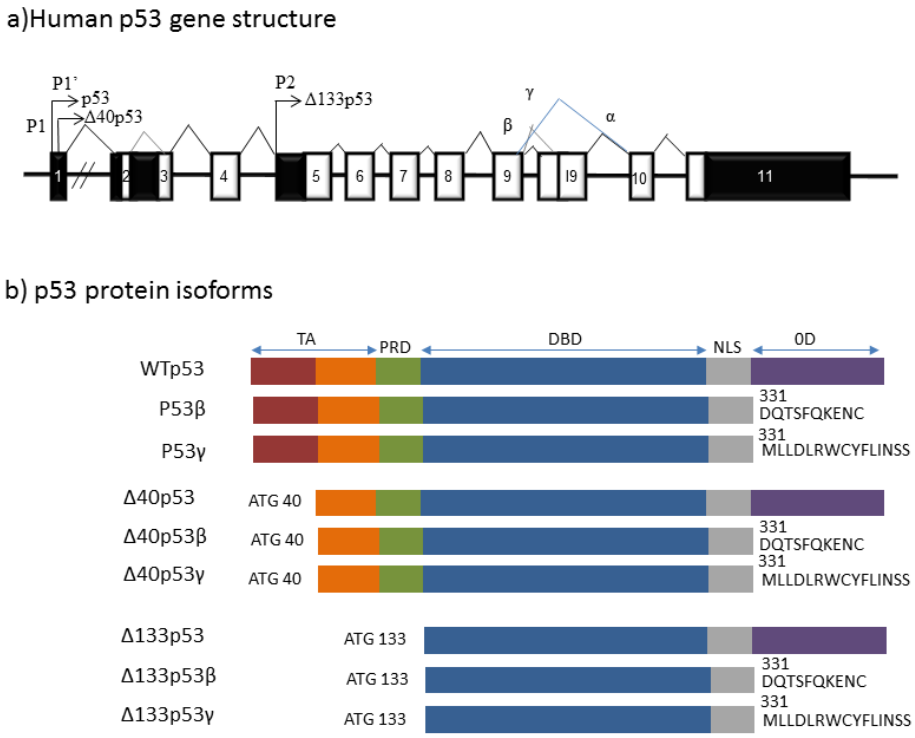

Figure 2 Schematic representation of a) Human p53 gene structure: alternative splicing (α, β, γ) and alternative promoters (P1, P1' and P2) are indicated. b) The p53 protein isoforms generated by alternative promoters and/or alternative splicing.

isoforms p53, p53β and p53γ can be generated by, where the p53β and p53γ isoforms without the oligomerization domain.

Thus, the p53 can generate 9 protein isoforms, indicated p53, p53β, p53γ, Δ133p53, Δ133p53β and Δ133p53γ due to alternative splicing of the intron 9 and usage of the alternative promoter in intron 4, and Δ40p53, Δ40p5 β, Δ40p53γ due to alternative splicing of the intron 9 and alternative initiation of translation or alternative splicing of the intron 2. However, new splice variants of p53 are discovery, p53ζ, p53Δ and p53ε, arising from alternative splicing of exon 6 and intron 9, respectively. [49]

p53 variant mRNA are expressed in several normal human tissues in a tissue-dependent manner, suggesting that the internal promoter and the alternative splicing of p53 can be regulated.

The human p73 gene is composed of 15 exons spanning over 80 000bp oh chromosome 1p36.3. **(figure 3 a)**

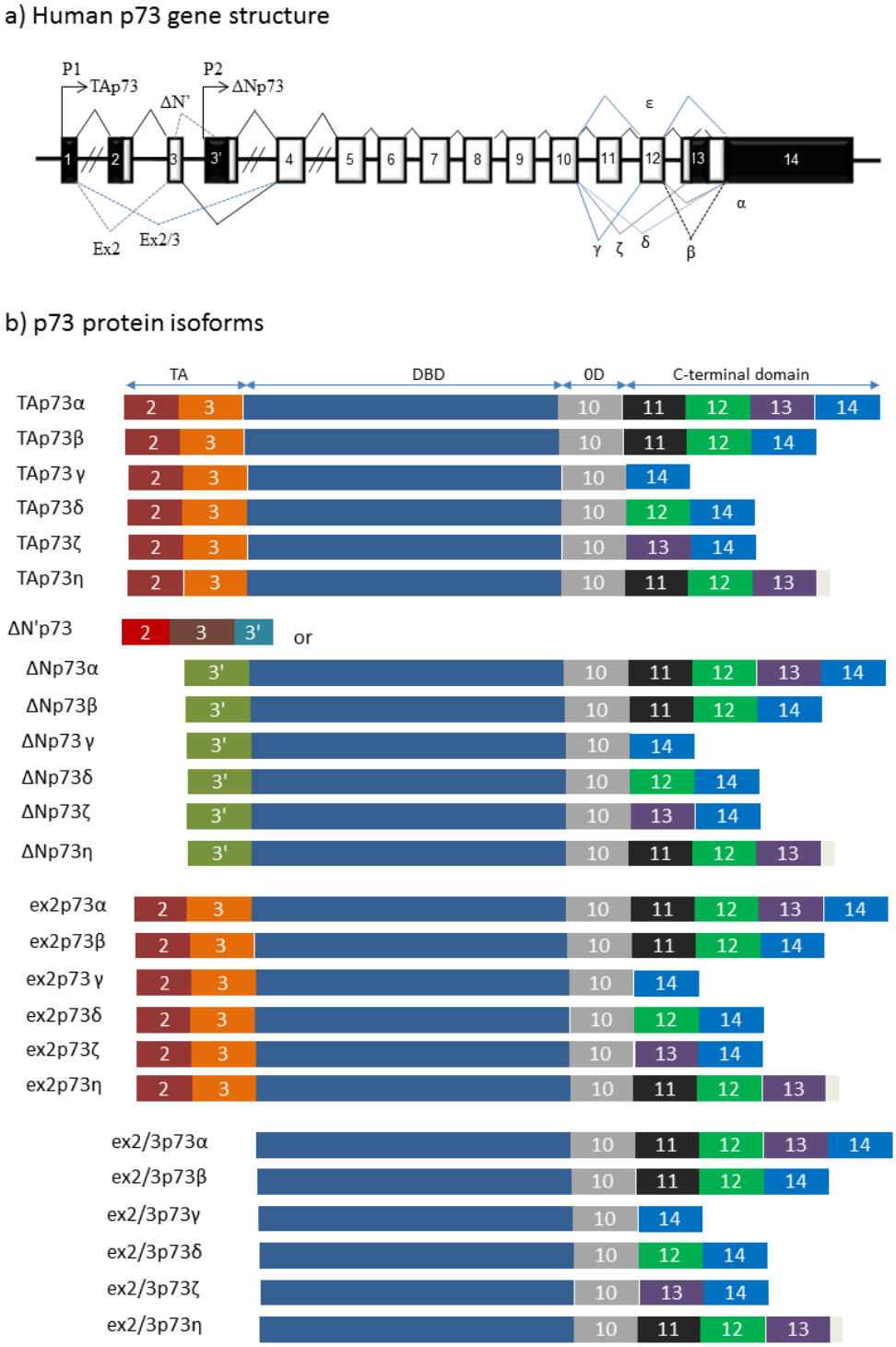

Figure 3 Schematic representation of a) Human p53 gene structure: alternative splicing (α, β, γ, δ, ζ, η) and alternative promoters (P1 and P2) are indicated. b) The p53 protein isoforms generated by alternative promoters and/or alternative splicing.

The p73 gene encodes at least seven alternatively spliced C-terminal isoforms (indicated α, β, γ, δ, ε, and ζ) and at least four alternatively spliced N-terminal isoforms initiated at different ATG. **(figure 3 b)** The p73 gene can be transcribed from alternative promoter in the intron 3 to produce an amino terminal truncated isoforms (ΔNp73) lacking of the transactivation domain, while the transactivating isoforms (TAp73) are generated by the activity of the promoter upstream of exon 1. Although the p73 gene encodes at least 35 mRNA variants, only 14 different protein isoforms have been described. The ΔN'p73 variant contains three first exons of Tap73, probably the translation is initiated from the first ATG located in exon 2 and it is finished at codon stop located in exon 3', leading to expression of a short p73 protein composed only of the N-terminal domain. The protein encoded by ΔN'p73 mRNA has not be identify. So, the p73 isoforms can be contain different part of the N-terminal domain, suggesting that they have different protein interaction and specific activities.

The TA isoforms can be bind specifically to DNA through p53RE and activate transcription of target genes inducing cell cycle arrest or apoptosis like p53. However p73 can bind DNA through response elements specific to p73 and different to p53RE.

The ΔN isoforms can be bind DNA through p53RE, but they have a dominant-negative effect over p53, p73 and p63 activities by competing for DNA binding sites or by direct protein interaction showing antiapoptotic acticity.[20,37] ΔNp73 isoforms can active transcription of gene target not induced by TA isoforms.

The human p63 gene is located on chromosome 3q27 and is composed of 15 exons spanning over 270 000 bp.**(figure 4 a)** The p63 can be transcribed from alternative promoters (P1 and P2) and express at least three alternative spliced C-terminal isoforms (α, β and γ).The transactivating isoforms (TA) are generated by the activity of promoter P1 upstream of exons 1, while the alternative promoter P2 in intron 3 leads to the expression of N-terminal truncated isoforms (ΔN) without transactivation domain. The p63 gene expresses for six mRNA which encode for six different protein isoforms: Tap63α, Tap63β, Tap63γ, ΔNp63α, ΔNp63β and ΔNp63γ.**(figure 4 b)** The isoforms TAp63, containing the N-terminal transactivation domain, are able to bind DNA through p53RE, activate transcription of target genes and thus induce cell cycle arrest or apoptosis, like p53. However TAp63 can bind DNA through response element (p63RE) to p63.[50] ΔNp63 isoforms also can bind DNA through p53RE and can have dominant-negative effect by either competing for DNA binding site or by direct protein interaction.[52] ΔNp63 isoforms can active specific gene targets not induced by TA isoforms. [53]

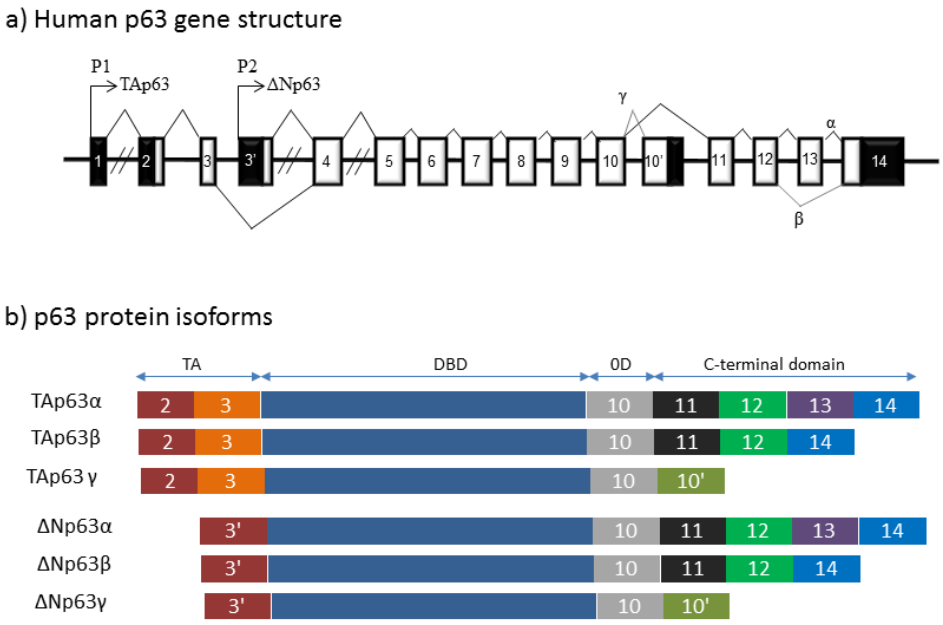

Figure 4 Schematic representation of a) Human p63 gene structure: alternative splicing (α, β, γ) and alternative promoters (P1 and P2) are indicated. b) The p53 protein isoforms generated by alternative promoters and/or alternative splicing.

1.4 Biological activity of p53 family protein isoforms

Though the p53 family proteins share similar domain structure and the TA isoforms can activate apoptosis in response to DNA damaging insults, the outcome of their ablation in vivo is strikingly different. Indeed, p63 and p73 are important in the regulation of *epidermal* and neuronal development respectively. **(figure 5).**

The p53 is frequently inactivated or mutated in over 50% of human tumors, while p73 and p63 are mutated in only 1% of human tumors, thus excluding them as classic Knudson-type tumor suppressor genes. [54,55] However, emerging evidence indicates that they may contribute to tumorigenesis. Unlike p53 null mice, which manifest increased susceptibility to spontaneous and

experimentally induced tumors, p63 and p73 loss does not result in increased tumorigenesis in vivo [56]

	Cell Cycle arrest	Apoptosis	Development
p53	+++	+++	-
ΔNp53	?	?	++
TAp73	++	+	+++
ΔNp73	-	-	+
TAp63	++	++	+++
ΔNp63	-	-	++

Figure 5 Schematic classification of the functions of p53 family proteins.

Genetic study have shown that p63 is essential for epidermal morphogenesis and limb development. ΔNp63 isoforms are expressed in the progenitor cell layers of skin, breast and prostate, while Tap63 isoforms are poorly detectable, indicating a different expression of p63 isoforms during normal cellular differentiation.[57] Recently, some studies demonstrate that TAp63 isoforms are the first to be expressed during embryogenesis and are very important for initiation of epithelial stratification.[58] TAp63 isoforms inhibit terminal differentiation and probably TAp63 isoforms must be counterbalanced by ΔNp63 isoforms to allow cells to respond to signals required maturation of embryonic epidermis and to differentiate.

In human, the *p63* gene usually is amplified in squamous cell in lung and cervical carcinomas, and TAp63 isoforms are expressed in most malignant lymphomas but ΔNp63isoforms are not expressed.

P63 null mice born alive but not survive more than a few days after birth. They have striking developmental defects: craniofacial malformations, limb truncations and fail to develop skin and other epithelial tissues. In human, germ line mutation of p63 are found and cause six rare autosomal dominant development disease: Ectrodactyly Ectodermal dysplasia–Clefting syndrome (EEC), Acro-dermato-ungual-lacrimal-tooth malformations (ADULT), Limb–Mammary Syndrome (LMS). Hay–Wells syndrome, also named AEC syndrome for Ankyloblepharon (partial or complete fusion of eyelids) and Ectodermal dysplasia-Clefting, Split-hand/foot malformations (SHFM) and Rapp–Hodgkin Syndrome.[59]

EEC and ADULT (ectrodactyly) syndromes result from missense mutation in the DNA binding domain of p63 that affect all p63 isoforms, while AEC (absence of ectrodactyly) [60] are cause

by missense mutation in exon 13 affecting only TAp63α and ΔNp63α. This suggest that TAp63α and ΔNp63α have a specific biological activities and are necessary to normal ectodermal development of specific organs.

The *p73* gene is expressed at very low level in all normal tissue. p73 gene frequently undergoes loss of heterozygosity in some tumors: lung, ovarian and neuroblastoma. However, the most common cancer specific alteration is an overexpression of p73 and not the loss of its function. [61] Studies show that expression of p73 in different stage of development of colon tumors is associated with poor outcome of disease. TAp73 and ΔNp73 are overexpressed in many tumors. In different human tumor, abnormal variation of p73 is observed. Since, in different part of the same tumor could be expressed different variant of p73 isoforms and this heterogenity reflect the biological heterogenity of tumor. Often the hallmark of tumor formation is the change of the balance between p73 isoform expression. ΔNp73 are relevant component of tumor-associated p73 expression, functionally overriding an accompanying increase of TAp73 expression. To date no syndrome in human associated with mutation of p73 has been found.

Mice p73 null die before 4 week of age with only 25% of them reaching adulthood [62]. At birth, p73 deficient mice manifest hippocampal dysgenesis due to massive apoptosis of sympathetic neurons in superior cervical ganglion, with approximately 40% of cell loss.[63]

Later on, they display hypersecretion of cerebrospinal fluid resulting in hydrocephalus, as well as runting, and abnormal social and reproductive behavior because of defects in pheromone detection. In addition, they have immunological problems characterized by chronic infections and inflammation.

These findings indicate the central role of p73 in the developing neuronal cells as well as in mature nervous system in the long-term maintenance of adult neurons.

During normal nervous system development, the antiapoptotic ΔNp73 isoforms have a prosurvival role in developing brain and sympathetic ganglia. In response to NGF withdrawal, the basal levels of ΔNp73 decline dramatically, thus allowing neurons to undergo cell death during nervous system develop. If the absence of ΔNp73 is rescued by ectopic expression of ΔNp73 isoform, neurons are protected from apoptosis.

ΔNp73 is an NGF-induced anti-apoptotic protein in sympathetic neurons and during development, neuronal survival is guaranteed by the availability of NGF, which in turn maintains the ΔNp73 levels high enough to inhibit the pro-apoptotic functions of both p53 and TAp63. **(figure 6 a)** On the other hand, once the levels of NGF becomes restrictive, neuronal cells are committed to cell death through down-regulation of ΔNp73 and augmented TAp63. Under these

circumstances, the antagonistic action of ΔNp73 is released, and the proapototic family members can elicit cell death by initiating mitochondrial apoptosis **(figure 6 b).**

The neuronal defects observed in the p73 knockout mice are a result of the absence of the ΔNp73 isoforms that normally block p53/TAp73/TAp63-mediated apoptosis in developing neurons.

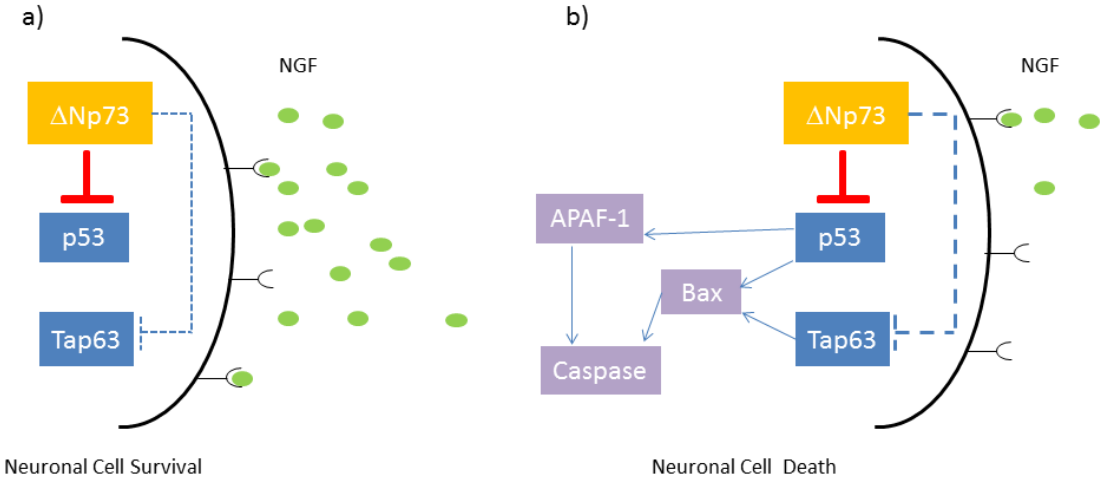

Figure 6. Regulation of developmental sympathetic neuronal survival and apoptosis by the p53 family members. The p53 protein family has been implicated in the death signaling following NGF withdrawal.

2 MATERIALS AND METHODS

2.1.1 Cell culture and reagents

Human osteosarcoma SAOS-2 with doxycycline-inducible expression of HA-TAp73α were cultured in Dulbecco's modified Eagle's and F12 medium (Gibco, Invitrogen), supplemented with 10% fetal bovine serum (FBS), 100 µg/ml penicillin and 100 µg/ml streptomycin (all Gibco, Invitrogen) and cultured at 37 C° with 5% CO_2.
To induce TAp73α expression, Saos-2- TAp73α cells were grown in the presence of doxycyclin (2 µg/ml) for 24 hours.

2.1.2 RNA isolation and qRT-PCR

Total mRNA was isolated using the RNeasy mini kit (Qiagen, Duesseldorf, Germany) following manufacturer recommendations. Total RNA was quantified using a NanoDrop Spectophotometer (Thermo Scientific, Delaware, USA) and used for cDNA synthesis using SuperScript Reverse Transcriptase (Promega, Fitchburg, WI, USA), according to the manufacturer's protocol. cDNA was subsequentially used for Real-Time PCR analysis (qRT-PCR). Each 25 µl reaction contained 2X SYBR-Green PCR Master Mix (Applied Biosystems), 0.125 µl MultiScribe Reverse Transcriptase (Applied Biosystems), 2 µl cDNA and the appropriate specific primers (0.5 µM, sequences available upon request). Amplification and fluorescence detection according to the manufacturer's instructions was performed using the ABI PRISM 7700 Sequence Detection System (Applied Biosystems, France).
The expression of each gene was defined from the threshold cycle (Ct), and relative expression levels were calculated using the 2-ΔΔCt method. The following primers were used: for hPGLS 5'- CAGACCACCCCCTCCTACAG -3'; rev hPGLS 5'- CTGCCTTGCCTTCTCCAGTT -3'; for hp21 5'-CACTGCCCTCCCATTACCTAG-3', rev hp21 5'-GAAGCTCAAGCATGGGAACAG-3'; for hActin 5'GTTGCTATCCAGGCTGTGCTA-3'; rev hActin 5'-AATGTCACGCACGATTTCCCG-3'.

2.1.3 Immunoblot analysis, antibodies and cell cycle analysis

Immunoblot analysis was performed using whole cell extracts obtained by lysing cell pellets with Triton Buffer (50 mM Tris-Hcl pH 7.5, 250 mM NaCl, 50 mM NaF, 1mM EDTA 1 pH 8, 0.1% Triton), supplemented with protease and phosphatase inhibitors. Proteins were separated by SDS-PAGE, transferred onto PVDF membranes and blocked with PBS-T (Phosphate-buffered saline and 0,1%Tween-20) containing 5% non-fat dry milk for one hour at room temperature (RT). The incubation with primary antibodies was performed for two hours at RT, followed by incubation with the appropriate horseradish peroxidase-conjugated secondary antibody. Detection was performed with ECL Western Blot Reagent (Perkin Elmer). Mouse monoclonal antibodies were from Covance (anti-HA), Sigma (actin), Santa Cruz (anti-p21). Anti-rabbit IgG or anti-mouse IgG horseradish peroxidase-conjugated antibodies were purchased by Perkin Elmer.
Quantification of sub-G1 population and cell cycle phase was performed by FACS analysis of propidium iodide-staining nuclei, carried out in a FACScan flow cytometer (Becton Dickinson, Heidelberg, Germany) using the CELLQuest software system.

2.2 METABOLOMISC AND LIPIDOMICS

2.2.1 Metabolite and Lipid extraction

One million cells per group (control and p73α-induced SAOS-2 cells) were exploited for subsequent metabolomics and lipidomics analyses. Samples were extracted following the protocol by D'Alessandro et al. [64]. In brief, cells were resuspended in 0.15 mL of ice cold ultra-pure water (18 MΩ) to lyse cell, then the tubes were plunged into a water bath at 37°C for 0.5 min. Samples were mixed with 0.6 mL of -20°C methanol and then with 0.45 mL chloroform. Subsequently, 0.15ml of ice cold ultra-pure water was added to each tube and vortexed every 5 mintues for 30 minutes. Tubes were then transferred to -20°C freezer for 2-8 h. An equivalent volume of acetonitrile was added to the tube and transferred to refrigerator (4°C) for 20 min. Samples with precipitated proteins were thus centrifuged for 10000 x g for 10 min at 4°C. Two phases were thus recovered, the upper hydrophilic phase (metabolites) and the lower hydrophobic phase (lipids), with cell membrane debris at the interface. Finally, samples from

separated phases were dried in a rotational vacuum concentrator (RVC 2-18 - Christ Gmbh; Osterode am Harz, Germany) and re-suspended in 200 µl of water, 5% formic acid and transferred to glass auto-sampler vials for LC/MS analysis.

2.2.2 Rapid Resolution Reversed-Phase HPLC

An Ultimate 3000 Rapid Resolution HPLC system (LC Packings, DIONEX, Sunnyvale, USA) was used to perform metabolite and lipid separation. The system featured a binary pump and vacuum degasser, well-plate autosampler with a six-port micro-switching valve, a thermostated column compartment. Samples were loaded onto a Reprosil C18 column (2.0mm×150mm, 2.5 µm - Dr Maisch, Germany) for metabolite and lipid separation.

Chromatographic separations were achieved at a column temperature of 30°C; and flow rate of 0.2 mL/min. For downstream negative ion mode (-) MS analyses, a 0–100% linear gradient of solvent A (10mM tributylamine aqueous solution adjusted with 15mM acetic acid, pH 4.95) to B (methanol mixed with 10 mM TBA and with 15 mM acetic acid, pH 4.95) was employed over 30 min, returning to 100% A in 2 minutes and a 6-min post-time solvent A hold. For downstream positive ion mode (+) MS analyses, a 0–100% linear gradient of solvent A (ddH_2O, 0.1% formic acid) to B (acetonitrile, 0.1% formic acid) was employed over 30 min, returning to 100% A in 2 minutes and a 6-min post-time solvent A hold.

For lipids the gradient program started with 100% solvent A (acetonitrile-methanol 99:1 (v/v) containing 5 mmolL-1 ammonium acetate) for 10 min. The mobile phase was linearly changed to 30% solvent B (methanol-water 80:20 (v/v) containing 5 mmolL-1 ammonium acetate) over 10 min, reached 40% solvent B in 15 min, and was maintained so for another 10 min, followed by a fast change to 100% solvent A in 5 min. At the end of gradient, the column was reconditioned with 100% solvent A for 10 min. The overall run time was 60 min. Column oven was 50°C and flow rate of 0.5 mL/min.

2.2.3 Untargeted Metabolomics: Mass Spectrometry: Q-TOF settings

Owing to the use of linear ion counting for direct comparisons against naturally expected isotopic ratios, time-of-flight instruments are most often the best choice for molecular formula

determination. Thus, mass spectrometry analysis was carried out on an electrospray hybrid quadrupole time-of flight mass spectrometer MicroTOF-Q (Bruker-Daltonik, Bremen, Germany) equipped with an ESI-ion source. Mass spectra for metabolite extracted samples were acquired both in positive and in negative ion mode. ESI capillary voltage was set at 4500V (+) (-) ion mode. The liquid nebulizer was set to 27 psi and the nitrogen drying gas was set to a flow rate of 6 L/min. Dry gas temperature was maintained at 200°C. Data were stored in centroid mode. Data were acquired with a stored mass range of m/z 50–1200. Automatic isolation and fragmentation (AutoMS^n mode) was performed on the 4 most intense ions simultaneously throughout the whole scanning period (30 min per run).

Calibration of the mass analyzer is essential in order to maintain an high level of mass accuracy. Instrument calibration was performed externally every day with a sodium formate solution consisting of 10 mM sodium hydroxide in 50% isopropanol: water, 0.1 % formic acid. Automated internal mass scale calibration was performed through direct automated injection of the calibration solution at the beginning and at the end of each run by a 6-port divert-valve.

2.2.4 Targeted metabolobomics and lipidomics: Multiple Reaction Monitoring (MRM)

Metabolites and lipids of interest were thus further tested for validation with multiple reaction monitoring (MRM), as previously reported [64]. Instrument set up, calibration curves and relative quantitations were performed against external standards from SIGMA Aldrich (Milan, Italy). Metabolites/lipids were directly eluted into a High Capacity ion Trap HCTplus (Bruker-Daltonik, Bremen, Germany). Mass spectra for metabolite/lipid extracted samples were acquired in positive and negative ion mode, as previously described [64]. ESI capillary voltage was set at 3000 V (+) ion mode. The liquid nebulizer was set to 30 psig and the nitrogen drying gas was set to a flow rate of 9 L/min. Dry gas temperature was maintained at 300 °C.

Data was stored in centroid mode. Internal reference ions were used to continuously maintain mass accuracy. Data were acquired at the rate of 5 spectra/s with a stored mass range of m/z 50–1500. Data were collected using Bruker Esquire Control (v. 5.3 – build 11) data acquisition software. In MRM analysis, m/z of interest were isolated, fragmented and monitored (either the parental or fragment ions) throughout the whole RT range. Validation of HPLC online MS-eluted metabolites was performed by comparing transitions fingerprint, upon fragmentation and

matching against the standards metabolites/lipids through direct infusion with a syringe pump (infusion rate 4 μl/min).

For lipid analyses, MS analysis was carried out in negative ion mode capillary voltage 2800V, nebulizer 45 psi and dry gas of 9 l/min, scan mode 100-1500 m/z. For sample injection, solutions were evaporated to dryness and reconstituted in an adequate volume of methanol:ethanol 1:1. Lipids extracts were prepared by dilution to a concentration of 5 pmol/L (where total phospholipids concentration was 2.5 pmol/L). Tandem mass spectrometry (MS/MS) is used for glycerophospholipid species structural characterization. Unambiguous species identification is done by analysis of the retention time and fragmentation pattern and comparative to those acquired from chemically defined standards (Avant Polar Lipids, Inc., Alabaster, Al.) [65].

2.2.5 Data elaboration and statistical analysis

In order to reduce the number of possible hits in molecular formula generation, we exploited the SmartFormula application within the MAVEN software package (Bruker Daltonics, Bremen, Germany), which directly calculates molecular formulae based upon the MS spectrum (isotopic patterns) and transition fingerprints (fragmentation patterns). This software generates a confidence-based list of chemical formulae on the basis of the precursor ions and all fragment ions, and the significance of their deviations to the predicted intact mass and fragmentation pattern (within a predefined window range of 5 ppm).

Triplicate runs for each group (TAp73α-induced vs non-induced controls) were exported as mzXML files and processed through MAVEN [66]. Mass spectrometry chromatograms were elaborated for peak alignment, matching and comparison of parent and fragment ions, and tentative metabolite identification (within a 20 ppm mass-deviation range between observed and expected results against the KEGG pathway database [67]). Relative quantitation and pathway representations were determined upon normalization against non-induced controls in a pathway-wise fashion. Data were further refined and plotted with GraphPad Prism 5.0 (GraphPad Software Inc.).

2.3 PROTEOMICS

2.3.1 Protein extraction and 2DE analyses

Cell lysis was performed in lysis buffer (7 mol/L urea, 2 mol/L thiourea, 4% CHAPS, protease inhibitor cocktail). The cell debris was removed by centrifugation (16,000 g, 20 min, 4°C) and samples were stored at -80°C. Protein concentration was determined using the 2-D Quant Kit (GE Healthcare, Little Chalfont, Buckinghamshire, UK).

A total of 8 2DE gels have been performed during the proteomic analysis of membrane proteins (4 technical replicates per group – TAp73α-induced and non-induced controls). Proteins were precipitated from a desired volume of each sample with a cold mix of tri-n-butyl phosphate/acetone/methanol (1:12:1) as described elsewhere [68]. After washing with the same solution, the pellet was air-dried and then solubilized in the focusing solution containing 7 M urea, 2 M thiourea, 2% (w/v) CHAPS ,40 mM Tris, , 0.1 mM EDTA (pH 8.5), 2% (v/v) protease inhibitor cocktail (Sigma-Aldrich). Proteins were subsequently reduced (10 mM tributylphosphine, 1 h) and alkylated (40 mM IAA, 1 h). To prevent over-alkylation, iodoacetamide (IAA) excess was destroyed by adding 10 mM DTE. Finally, a new precipitation step was performed as describe before.

Six hundred μg of protein samples were resuspended in 300 μL of isoelectric focusing buffer (7M urea, 2M thiourea, 4% CHAPS, 0.2% Bio-Lyte 3/10 ampholyte) and absorbed into 17 cm ReadyStrip^{TM} IPG strips (Bio-Rad, Hercules, CA, USA) following the manufacturer's directions. Isoelectric focusing was performed on a Protean IEF Cell (Bio-Rad, Hercules, CA, USA) with the following program: 200 V for 1 hour, 500 V for 1 hour, 1000V for 1 hour 3000 V for 1 hour, 5000 V for 60000 VH.

For the second dimension, the IPG strips were equilibrated for 30 min in a solution containing 6 M urea, 2% (w/v) SDS, 20% (v/v) glycerol, and 50 mM Tris-HCl (pH 8.8) under gentle agitation. Then, IPG strips were overlaid onto 12% SDS-PAGE gels and electrophoretic run was performed at a constant current (10 mA for 60 min, followed by 40 mA until the run was completed). During the whole run, the temperature was set at 10°C.

Proteins were visualized through sensitive Coomassie Brilliant Blue G-250 stain [69].

2.3.2 Statistical analyses and trypsin digestion

Stained gels were digitalized using ChemiDoc™ XRS+ System with Image Lab™ Software (Bio-Rad, Hercules, CA) and image analysis was performed using Progenesis SameSpot software v.2.0.2733.19819 software package (Nonlinear Dynamics, New Castle, UK). Each gel was analyzed for spot detection and background subtraction. Within-group comparison of protein spot numbers was determined by repeated measures analysis; thus, the arithmetic mean of the total spot number (standard deviation (SD) was considered). Among-group comparisons were determined by ANOVA (Analysis of Variance) procedure in order to classify sets of proteins that showed a statistically significant difference with a confidence level of 0.05. Moreover, protein spots matching across all the replica maps were selected and analyzed by MS/MS.

Spots from 2-DE maps of biological interest ($p<0.05$) were carefully excised from the gel and subjected to in-gel trypsin digestion according to Shevchenko et al. [70] with minor modifications. The gel pieces were swollen in a digestion buffer containing 50 mM NH4HCO3 and 12.5 ng/mL trypsin (modified porcine trypsin, sequencing grade, Promega, Madison, WI) in an ice bath. After 30 min, the supernatant was removed and discarded; then 20 μL of 50mM NH4HCO3 were added to the gel pieces, and digestion was allowed to proceed overnight at 37 °C. The supernatant containing tryptic peptides was dried by vacuum centrifugation. Prior to mass spectrometric analysis, the peptide mixtures were redissolved in 10 μL of 5% FA (formic acid).

2.3.3 Phosphoproteomics analyses

TiO_2 enrichment and CID/ETD-analysis of phosphopeptides were performed as previously reported [71, 72].

Cell lysis was performed in lysis buffer (7 M urea, 2 M thiourea, 4% (w/v) CHAPS, 50mM Tris, 0.1 mM EDTA (pH 8.5), 2% (v/v) protease inhibitor cocktail (Sigma-Aldrich, Basle, Switzerland), 2mM orthovanadate). Samples were then centrifuged (16,000×g, 15 min, 4 °C) to remove cellular debris. The supernatant was transferred to a new Eppendorf tube and protein estimation was subsequently performed using a 2Dquant kit (GE Healthcare, Little Chalfont, Buckinghamshire, UK) 200 μg of protein was precipitated using a cold mix of tri-n-butyl

phosphate/acetone/methanol (1:12:1) as described elsewhere [68] and resuspended in 7 M urea, 2 M thiourea, 50 mM Tris–HCl (pH 8.8) to a final concentration of 2 μg/μL. Proteins were reduced (DTT 2 mM, 30 min) and alkylated (8 mM iodacetamide, 1 h). Finally, to prevent overalkylation, iodoacetamide (IAA) excess was neutralized by adding 2 mM DTE. A new precipitation step was performed and sample was resuspended in 50 mM ammonium bicarbonate containing 1 M urea and 0.1% SDS. Trypsin was added to a final protease:protein ratio of 1:50 (w/w) and incubated overnight at 37 °C.

Prior to phosphopeptide enrichment, the digested samples were desalted using ZipTip C18 pipette tips (Millipore, Billerica, MA, USA) following the manufacturer's directions. Purification of phosphopeptides was then performed according to Larsen et al. [72]. Briefly, tryptic peptides were diluted 5-fold in dihydroxybenzoic acid (DHB) buffer [350 mg/mL DHB, 80% (v/v) ACN, 2% (v/v) TFA] and applied to TiO_2 beads (200 μg) pre-equilibrated in 50% ACN. The sample was then washed once in DHB buffer, before being washed two times with wash buffer [80% ACN (v/v), 2% TFA (v/v)] to remove the DHB. The sample was finally eluted with 25 μL of 2.5% ammonium hydroxide solution (pH≥10.5) and immediately neutralized with 2.5 μL of formic acid. All buffers used ultrapure water and were made fresh on the day of experimentation.

2.3.4 Mass spectrometry-based identification of proteins and phosphopeptides

Mass spectrometric procedures for proteomics and phosphopeptide analyses were performed as previously described.

To provide a larger list of phosphorylation sites, the TiO_2-enriched samples were analyzed using a split-free nano-flow liquid chromatography system (EASY-nLC II, Proxeon, Odense, Denmark) coupled to a 3D-ion trap (model AmaZon ETD, Bruker Daltonik, Germany) equipped with an online ESI nano-sprayer (the spray capillary was a fused silica capillary, 0.090mm o.d., 0.020mm i.d.). For all experiments, a sample volume of 15 μL was loaded by the autosampler onto a homemade 2 cm fused silica precolumn (100 μm I.D.; 375 μm O.D.; Reprosil C18-AQ, 5 μm, Dr. Maisch GmbH, Ammerbuch-Entringen, Germany). Sequential elution of peptides was accomplished using a flow rate of 300 nL/min and a linear gradient from Solution A (2% acetonitrile; 0.1% formic acid) to 50% of Solution B (98% acetonitrile; 0.1% formic acid) in 40 min over the precolumn in-line with a homemade 15 cm resolving column (75 μm I.D.; 375 μm O.D.; Reprosil C18-AQ, 3 μm, Dr. Maisch GmbH, Ammerbuch-Entringen, Germany). To

identify phosphorylation sites, two types of peptide fragmentation were carried out in parallel in the mass spectrometer: (i) Collision Induced Dissociation (CID); (ii) Electron Transfer Dissociation (ETD). When CID was used a MS2 was automatically performed on the three most intense MS ions, and MS3 was triggered if one of the top three MS2 peaks corresponded with neutral loss of 98.0, 49.0, 32.7 m/z. For ETD experiments the reaction time was set to 100 ms using a reactant ICC of 500000 allowing a maximum accumulation time for the reactant ion of 10 ms. A detailed description of the ETD setup of the ion trap instrument including the generation of the reagent anion of fluoranthene was given previously.[73] The acquisition parameters for the instrument were as follows: dry gas temperature, 220 °C; dry gas, 4.0 L/min; nebulizer gas, 10 psi; electrospray voltage, 4000 V; high-voltage end-plate offset, −200 V; capillary exit, 140 V; trap drive: 63.2; funnel 1 in, 100 V out 35 V and funnel 2 in, 12 V out 10 V; ICC target, 200000; maximum accumulation time, 50 ms. The sample was measured with the "Enhanced Resolution Mode" at 8100 m/z per second (which allows mono isotopic resolution up to four charge stages) polarity positive, scan range from m/z 300 to 1500, 5 spectra averaged, and rolling average of 1. The "Smart Decomposition" was set to "auto". Acquired ETD/CID spectra were processed in DataAnalysis 4.0, and deconvoluted spectra were further analyzed with BioTools 3.2 software and submitted to Mascot search program (in-house version 2.2, Matrix Science, London, UK). The following parameters were adopted for database searches: NCBInr database (release date 22/10/2011; 15 670 865 sequences; 5 387 755 057 residues); taxonomy=mammalia; peptide mass tolerance of ±0.3 Da; fragment mass tolerance of ±0.3 for CID ions and of ±1.3 Da for ETD ions; enzyme specificity trypsin with 2 missed cleavages considered; fixed modifications: carbamidomethyl (C); variable modifications: oxidation (M), phosphorylation (STY). Phosphopeptide identifications were accepted if the Mascot score was over the 95% confidence limit based on the "identity" score of each peptide. A delta ion score was calculated of all phosphopeptides containing more than one serine, threonine or tyrosine residues by taking the difference between the two top ranking Mascot ion scores. Phosphorylation site assignments with a delta score >5 were automatically accepted.[74] All fragmentation spectra with delta score ≤5 were manually inspected as to whether the phosphorylation sites were unambiguously determined or not.

3 RESULTS AND DISCUSSIONS

In order to evaluate the TAp73-dependent signaling, we utilized a subclone of the human osteosarcoma SAOS-2 cell line (p53 null cells) where the exogenous expression of HA-TAp73α is under control of a doxycycline responsive promoter. Upon 24 h of doxycycline treatment, the expression of TAp73α and its transcriptional target gene p21 is increased. The ectopic expression of TAp73α is able to induce cell cycle arrest or apoptosis within 48 h from doxycyline induction.9 Since in the present study we were interested in investigating the events leading to TAp73α-driven apoptosis, we analyzed the cell cycle profile of the cells 24 h from TAp73α induction. We confirmed that this time frame is adequate for further omics analyses in that early evidence of cell cycle arrest in G2/M phase and slight increases in the percentage of apoptotic cells were already visible at 24 h from the induction **(Fig. 7)**.

3.1 PROTEOMISC AND PHOSPHOPROTEOMICS ANALYSIS

Proteomics analysis revealed that the induction of TAp73α expression resulted in the up-regulation of 15 and down-regulation of 9 protein spots. Results are reported in **Table 1**, along with the indication of the extended protein name, theoretical MW and p*I*s, gene identifiers (NCBI gi), and identification details (the number of matched peptides and MASCOT scores). Distribution of protein spots in the control (left panel) and in the TAp73α–induced (right panel) SAOS-2 cells is showed on 2DE maps in **Figure 8.**

First of all, it is worthwhile noting that we assayed cells at 24 h after induction of TAp73α. This time frame is indeed sufficient to observe the induction of direct target genes of TAp73 transcriptional activity (Figure 1A) and early biological responses (such as cell cycle arrest, as reported above, Figure 1B). Since TAp73α is expressed roughly already at 8−12 h from induction in the Tet-On doxycycline-inducible SAOS2 cell line,11 some of the observed changes at the proteomics level might be also attributable to early indirect transcriptional effects of TAp73α activation.

Differentially-expressed proteins could be further divided on the basis of their biological activity, including:

a) proteins involved in p73 protein stabilization and in the regulation of its activity;

b) proteins involved in p73 degradation and protein turn-over;

c) proteins reflecting an active transcriptional state upon TAp73α–induction;

d) proteins linked to metabolism.

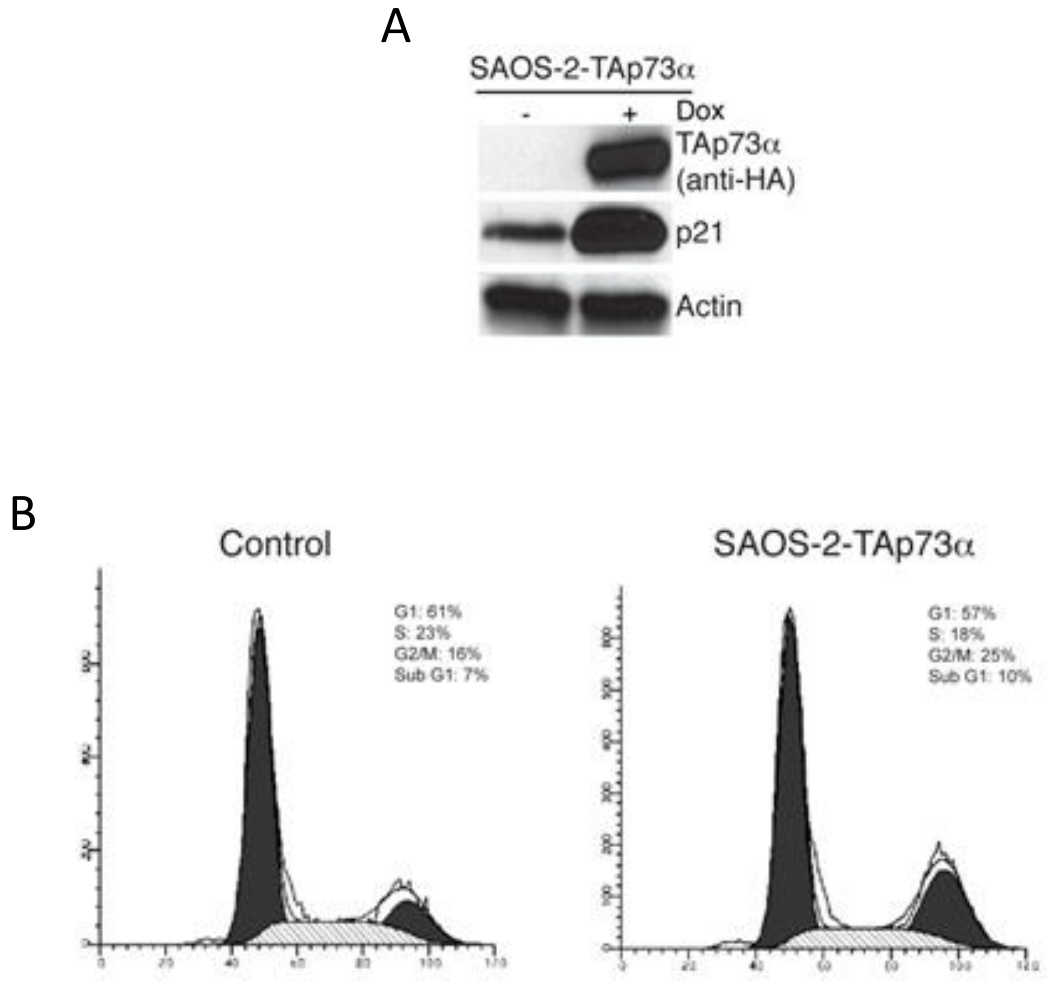

Figure 7. Human osteosarcoma SAOS-2 cells (SAOS-2-TAp73α) with doxycycline-inducible expression of HA-TAp73α were grown in the presence of doxycyclin (2 μg/ml) for twenty-four hours. **A)** Whole cell extracts of untreated and treated cells were utilized for western blot analysis using the antibodies to the indicated proteins. **B)** SAOS-2-TAp73α treated and untreated cell were subjected to FACS analysis. The percentage of sub G1, G1, S and G2/M cells is reported.

Table 1. Mass Spectrometry-Based Identification of Differentially Espressed Proteins upon Tap73α induction

Spot No.	Protein ID	Mr, Da Theor/exper	pI Theor/exper	NCBI GI No.	No. Of peptides	Mascot score	Fold Change
			Overexpressed in SAOS-2 Tap73α-induced				
230	90kDa heat shock protein	83584/85600	4.97/4.85	gi|306891	6	226	3
494	45 kDa calcium-binding protein	41895/55800	4.67/4.5	gi|18699732	2	92	3.5
	coiled-coil domain containing 97	39265/55800	4.5/4.5	gi|16418351	2	90	
	mitochondrial dihydrolipoamide succinyltransferase	49000/55800	9.01/4.5	gi|499719	2	84	
	UV excision repair protein RAD23 homologue A variant	41402/55800	4.66/4.5	gi|62089006	4	55	
591	Calumenin	37164/50000	4.47/4.3	gi|2809324	4	141	1.5
859	Serine/arginine-rich splicing factor 1 isoform 1	27842/36150	10.37/5.3	gi|5902076	4	162	1.8
874	Tubulin folding cofactor B	27663/35600	5.14/5	gi|2343185	5	91	1.5
	Microtubule-associated protein RP/EB family member 1	30151/35600	5.02/5	gi|6912494	12	197	

909	coatomer protein complex, subunit epsilon	34688/34300	4.97/5	gi|119605162	20	148	1.6
938	14-3-3 protein epsilon	29326/31300	4.63/4.6	gi|5803225	16	2100	1.7
975	14-3-3 protein epsilon	29326/31300	4.63/4.6	gi|5803225	2	240	1.8
987	Prohibitin	29843/30000	5.57/5.7	gi|4505773	5	181	1.5
	proteasome beta 7 subunit	30260/30000	7.57/5.7	gi|62898273	3	91	
	6-phosphogluconolactonase	27815/30000	5.70/5.7	gi|6912586	7	134	
1118	HSPC029	25329/25800	4.89/4.7	gi|5114051	3	266	1.6
	proteasome subunit Y	25527/25800	4.80/4.7	gi|558528	4	141	
1324	RNA polymerase II subunit	17203/17500	4.5/4.3	gi|1017823	3	236	1.5
1439	PSMC3	45507/49900	5.39/5.1	gi|48145579	54	724	1.6
	α-tubulin	50810/49900	5.02/5.1	gi|37492	2	200	
1454	mitochondrial ATP synthase, H+ transporting F1 complex β subunit	48083/50000	4.95/5.0	gi|89574029	8	567	2
	β-tubulin 4	50240/50000	4.75/5.0	gi|338695	4	147	
	p48	41470/50000	5.09/5.0	gi|904032	3	130	
1460	Smooth muscle myosin alkali light chain (Myosin light polypeptide 6)	17772/17000	4.57/4.2	gi|467828	2	112	1.7
1478	Protein disulfide isomerase-related protein 5	46512/50200	4.95/5.1	gi|1710248	18	693	1.7

	Dynactin subunit 2	44906/50200	5.06/5.1	gi|5453629	13	537	
	ATP synthase subunit beta, mitochondrial precursor	56525/50200	5.26/5.1	gi|32189394	18	458	
	Tat binding protein 1, TBP-1=transcriptional activator	49322/50200	5.08/5.1	gi|263098	10	258	
	p48	41470/50200	5.08/5.1	gi|904032	3	156	
	Tat binding protein 7, TBP-7 = transcriptional activator	51633/50200	5.52/5.1	gi|263099	7	90	
	Overexpressed in SAOS-2 Tap73α non-induced controls						
387	Plastin-3 isoform 1	71279/79000	5.41/5.75	gi|7549809	34	1022	1.5
489	Alpha-tubulin	50810/51000	5.02/5.1	gi|37492	43	998	1.5
	vimentin	53738/51000	5.03/5.1	gi|340219	9	302	
596	chaperonin (HSP60)	61157/61900	5.70/5.7	gi|306890	2	72	1.7
638	actin	42480/48000	5.23/5.1	gi|178027	3	93	1.7
649	Deaminase a,adenosine	41009/48000	5.62/5.7	gi|224877	5	227	1.7
998	prosomal RNA-binding protein p27K	27838/31900	6.34/6.3	gi|446773	12	1082	
	Enoyl-CoA hydratase	31807/31900	8.34/6.3	gi|1922287	10	394	
1199	not identified						1.9
1231	ribosomal protein L12	17979/19000	9.48/5.1	gi|4506597	2	94	1.5
1441	Mitochondrial ribosomal protein L7/L12	21593/21000	9.01/5.3	gi|1313962	3	154	1.8

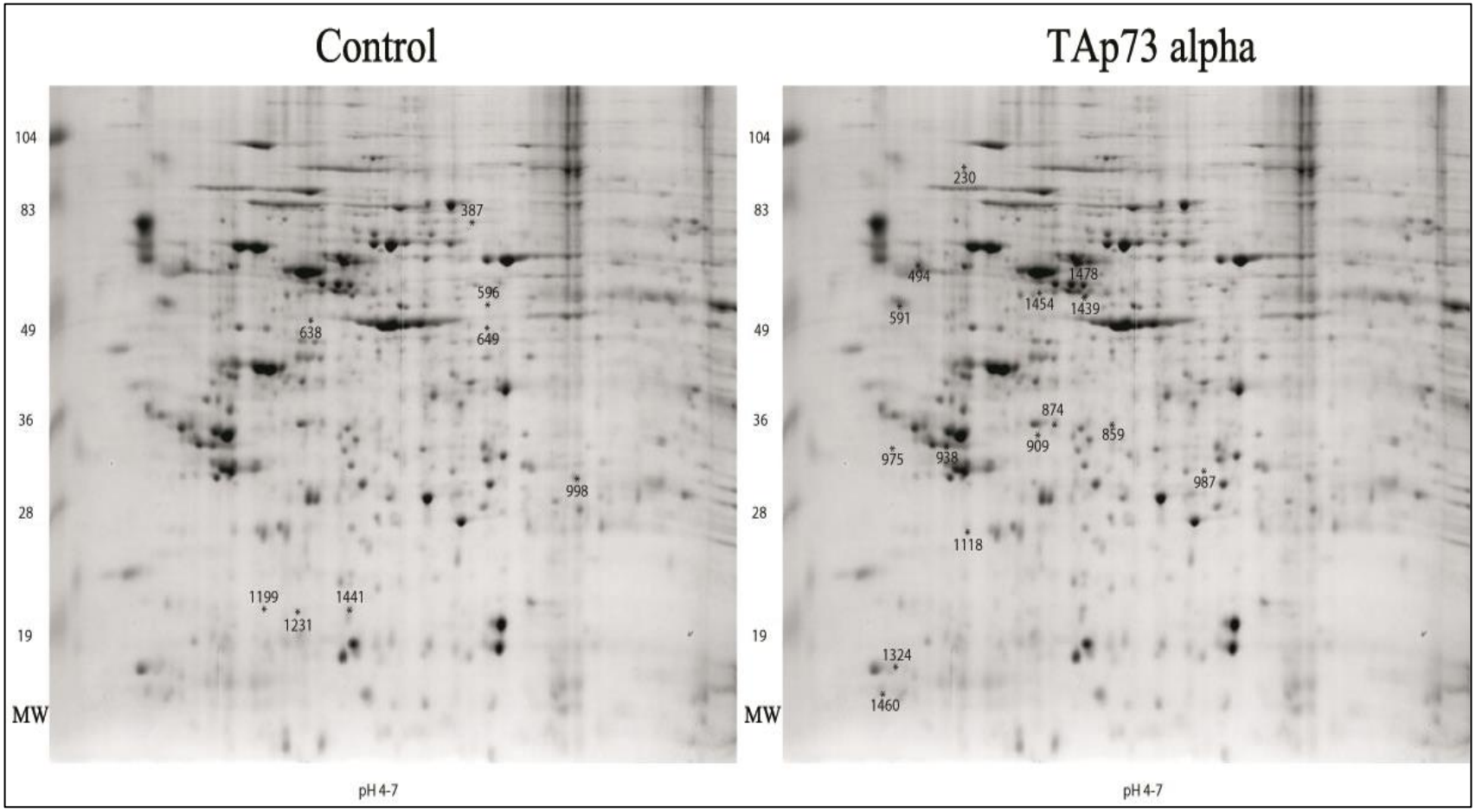

Figure 8. 2DE maps of non-induced controls (left panel) versus TAp73α-induced SAOS-2 cells. Spot numbers indicate differentially expressed proteins (p<0.05 ANOVA) upon statistical analyses through Progenesis Samespots, and relate to protein identifications reported in **Table 1.**

3.1.1 Regulation of p73 activity

We found that the 90kDa heat shock protein (HSP90 - spot n. 230 – **Table 1**) is up-regulated in TAp73α-induced cells. This phenomenon might be related to stabilization of the p73 protein through a mechanism conserved within the p53/p63/p73 protein family. Indeed, accumulation of the p73-homolog p53 results from ATM kinase-mediated phosphorylation of p53 at serine 15 or rather by HSP90-binding to wild type p53 [75]. Inhibition of HSP90-p53 interaction by geldanamycin completely prevented p53 accumulation in ATM-deficient cells [75]. Analogous mechanisms could contribute to the stabilization and accumulation of newly-expressed TAp73α.

Another protein whose expression is induced in TAp73α-expressing is 14-3-3 protein ε (spots n. 938 and 975 – **Table 1**). Several publications suggest that activation of p53 following DNA damage directly up-regulates the levels 14-3-3σ, and that this process is critical for maintaining the G2/M checkpoint [76, 77]. The interactions between p53 and 14-3-3 are complex, and likely to be at least partially cell type specific. For example, 14-3-3σ and other 14-3-3 isotypes, including 14-3-3ε have been reported to directly bind to p53 itself [77, 78], increasing the DNA-binding function and activity of p53 as a transcription factor. However, p53 activation depends upon dephosphorylation and binding to 14-3-3 proteins [77]. Again, the up-regulation of 14-3-3 protein ε in TAp73α-induced cells is suggestive of further shared similarities between p53 and p73 activation cascades.

3.1.2 Protein degradation and ER-stress

Protein degradation determines the outcome of many cellular physiological processes. Degradation of proteins by the proteasomes occurs via various and tightly-regulated pathways, the most extensively studied one being the ubiquitin–26S proteasome pathway [79].

The proteasomal degradation of the tumor suppressors p73 is regulated by both poly-ubiquitination (a mechanism that is inhibited by the promyelocytic leukemia (PML) protein [80, 81]) and by an ubiquitin-independent process [82, 83]. Unlike p53, p73 is not targeted for ubiquitinylation by the E3 ubiquitin ligase MDM2 [84, 85].Hereby, we could find an up-regulation of proteasome 26S (spot n. 1439) and TAT-binding protein 1 (an ATPase of 19S regulatory particles of the 26S proteasome [86] – spot n. 1478) upon induction of the expression of TAp73α (**Table 1**). In addiction, we could observe up-regulation of spot n. 987 in the

TAp73α-induced group, also identified as proteasome 20S subunit beta 7 (**Table 1**). Overall, these findings are suggestive of a likely protein turn-over upon p73 induction, a process that might result in a negative feedback loop towards homeostasis of the levels of p73 protein itself. Another tentative explanation stems from increased rates of protein degradation through the proteasome system under conditions of endoplasmic reticulum (ER) stress [81, 82], a condition that is known to be induced by TAp73α through a Scotin-mediated pathway [11]. Misfolding of proteins is associated with ER stress [81, 82] and hereby indirectly documented by the overexpression of protein disulfide isomerase 5 (PDIA5 – spot n. 1478 in **Table 1**) in TAp73α-induced cells. Indeed, PDIA5 is an ER enzyme that catalyzes the rearrangement of disulfide bonds between cysteine residues within proteins during folding. This allows proteins to quickly find the correct arrangement of disulfide bonds in their fully folded state, which makes PDIA5 a catalyst of proper protein folding that responds to ER stress stimuli [83].

In line with the posited hypothesis about proteomics changes reflecting p73α involvement in ER-stress, the p73-induced up-regulation of protein UV excision repair protein RAD23 homolog A (spot n. 494 – **Table 1**) can be related to DNA damage responses, ER stress and protein degradation [84]. The DNA repair protein RAD23 has been shown to inhibit degradation of specific substrates in response to DNA damage, including the associated nucleotide excision repair protein XPC thereby stimulating DNA repair in a mouse model [84]. The RAD23 homolog MIF1 binds to the 19S regulatory subunit of proteasome 26S and could play a role in the translocation of the 26S proteasome towards the ER-membrane, thereby enhancing ER-associated protein degradation [85]. It is at least worth noting that another protein was identified under the spot n. 494, namely 45 kDa calcium-binding protein, a protein that is involved in the regulation of calcium-dependent activities in the endoplasmic reticulum lumen or post-ER compartment.66 Consistently, ER-stress induced by p73 proteins follows a Scotin/caspase-dependent pathway [9, 11, 17, 86, 87].

Further clues to the p73α involvement in DNA damage repair, proteasome-dependent degradation stem from differential phosphoproteomics results (**Table 2**).

Phosphorylation of the ubiquitin fusion-degradation 1like protein at Ser299 (uniquely found in the TAp73α expressing cells -**Table 2**) is associated with inactivation of the pathways leading to DNA-damage repair and mTOR signaling occurring during mitosis or in response to ATM activation [88]. Connections between the mTOR-p73 signaling axis are not novel [89-91]. In the present study, additional supporting evidence is provided by phosphorylation at Ser250 of the proteasome subunit alpha type-3 (only present in the non-induced cells - **Table 2**), a post

translational modification that triggers inhibition of proteasome activity in response mTOR [92] and MAPK [93] signaling. Analogous considerations can be made for microtubule associated protein 4, phosphorylated at Ser280 in non-induced cells (**Table 2**), which is associated with cytokinesis during mitosis [94]. On the other hand, the up-regulation of microtubule-associated protein RP/EB family member 1 (MAPRE1 - up-regulated in TAp73α-induced cells – spot n. 874 in **Table 1**) was unexpected, since both p53 and p73β have been reported to inhibit transcription of this protein [95]. This might reflect differential p73 isoform-specific downstream regulation of target genes or rather differential PTM to this protein upon TAp73α-induction, causing spot displacement on the 2D map at the *pI*-level. Indeed, most of the pro-mitotic protein-protein interactions are modulated by phosphorylations. For example, MAPRE1 is known to interact with the stromal interaction molecule 1 (GOK), targeting to the growing microtubule plus ends [96] and promoting mitosis [97]. GOK is a Ca^{2+} sensor that resides in the ER and, upon Ca^{2+} depletion, it migrates to the membrane to trigger calcium release. Phosphorylation at Ser257 of GOK (**Table 2**) was peculiar of the non-induced group.

Table 2 – Phosphopeptidomics analyses of TAp73α-induced SAOS-2 cells

Phosphopeptides unique to TAp73 α-induced
Ubiquitin fusion-degradation 1 like protein
m/z 689.2604 **FVAFSGEGQ<u>S</u>LR + Phospho (ST)** (Mascot score: 47, NL)
Peptides unique to non-induced controls
GOK
m/z 703.2812 **AEQ<u>S</u>LHDLQER + Phospho (ST)** (Mascot score: 46, ETD)
Human elongation factor-1-delta
m/z 501.8514 **ATAPQTQHV<u>S</u>PMR + Phospho (ST)** (Mascot score: 45, ETD)
huMCM2
m/z 658.5643 **GLLYD<u>S</u>DEEDEERPAR + Phospho (ST)** (Mascot score: 51, ETD)

Microtubule-associated protein 4

m/z 814.4000 **DME<u>S</u>PTKLDVTLAK + Phospho (ST)** (Mascot score: 53, NL)

Proteasome subunit alpha type-3

m/z 868.2320 **ESLKEEDE<u>S</u>DDDNM.- + Phospho (ST)** (Mascot score: 53, ETD)

Translation initiation factor IF2

m/z 705.2633 **NKPGPNIE<u>S</u>GNEDDDASFK + Phospho (ST)** (Mascot score: 41, ETD)

Uncharacterized protein C12orf4

m/z 893.0097 **DAEASLAAVK<u>S</u>GEVDLHQLASTWAK + Phospho (ST)** (Mascot score: 43, ETD)

Shared phosphopeptides

60S acidic ribosomal protein P1

m/z 1023.2906 **KEE<u>S</u>EESDDDMGFGLFD.- + Oxidation (M); Phospho (ST)** (Mascot score: 69, NL)

Calnexin

m/z 754.7977 **AEEDEILNR<u>S</u>PR + Phospho (ST)** (Mascot score: 74, ETD)

eIF-3 p110 subunit

m/z 584.8919 **QPLLL<u>S</u>EDEEDTKR + Phospho (ST)** (Mascot score: 76, ETD)

hCG1817324, isoform CRA_a

m/z 579.5674 **A<u>S</u>M<u>S</u>GELRS<u>S</u>GNQR + Oxidation (M); 3 Phospho (ST)** (Mascot score: 47, ETD)

Hematological and neurological expressed 1 protein

m/z 569.2384 **RN<u>S</u>SEASSGDFLDLK + Phospho (ST)** (Mascot score: 88, ETD)

Hepatoma-derived growth factor

m/z 502.5566 **AGDLLEDSPKRPK + Phospho (ST)** (Mascot score: 74, NL; 67, ETD)

Heterogeneous nuclear ribonucleoprotein D0B

m/z 684.5732 **IDASKNEEDEGHSNSSPR + Phospho (ST)** (Mascot score: 120, ETD)

Heterogeneous nuclear ribonucleoprotein H

m/z 588.8542 **HTGPNSPDTANDGFVR + Phospho (ST)** (Mascot score: 109, ETD)

HSPC121

m/z 795.3309 **WLDESDAEMELR + Oxidation (M); Phospho (ST)** (Mascot score: 40, ETD)

m/z 795.2997 **WLDESDAEMELR + Oxidation (M); Phospho (ST)** (Mascot score: 46, NL)

HSR1 protein

m/z 544.9510 **REEQTDTSDGESVTHHIR + Phospho (ST)** (Mascot score: 82, ETD)

Nucleolin

m/z 492.2147 **LELQGPRGSPNAR + Phospho (ST)** (Mascot score: 68, ETD)

Protein transport protein Sec61 subunit beta

m/z 617.2425 **PGPTPSGTNVGSSGRSPSK + Phospho (ST)** (Mascot score: 90, ETD)

Ribonucleoprotein La

m/z 602.2233 **FASDDEHDEHDENGATGPVKR + Phospho (ST)** (Mascot score: 94, ETD)

SEPT2 protein

m/z 629.9698 **IYHLPDAESDEDEDFKEQTR + Phospho (ST)** (Mascot score: 61, ETD)

SEPT9 protein

m/z 445.2013 **HVDSLSQRSPK + Phospho (ST)** (Mascot score: 55, ETD)

3.1.3 Transcription regulation by TAp73

The quality of proteomics results is also confirmed by evidences supporting the role of p73 as a transcriptional activator. This assumption is also underpinned by increased levels of RNA pol II in TAp73α-induced SAOS-2 cells (spot no. 1324 – **Table 1**).

We also observed differential expression of splicing factors, including Serine/arginine-rich splicing factor 1 isoform 1 (spot n. 859 in TAp73α-induced cells – **Table 1**) and several heterogeneous nuclear ribonucleoproteins (**Table 2**). This is relevant in the light of splicing factors regulating apoptosis through alternative processing of pre-mRNA of apoptotic players [98].

Other than modulating transcription and mRNA splicing, TAp73α appeared to modulate also protein translation. We found indeed the up-regulation of eIF-3 (HSPC029 in spot n. 1118 in **Table 1**), an eukaryotic initiation factor which associates with the 40S ribosome and facilitates the recruitment of eIF-1, eIF-1A, eIF-2/GTP/methionyl-tRNAi and eIF-5 to form the 43S preinitiation complex (43S PIC). The eIF-3 complex stimulates mRNA recruitment to the 43S PIC and scanning of the mRNA for AUG recognition [99]. Mitogenic stimulation leads to mTOR and RPTOR-dependent phosphorylation and release of RPS6KB1 and binding of EIF4B to eIF-3 [100]. However, phosphorylations to Ser133 of human elongation factor-1-delta and to Ser214 of translation initiation factor IF2 (EIF1D and eiF5B, respectively - only detected in non-induced controls – **Table 2**) are necessary for human spindle assembly at mitotic checkpoints [100, 101] and mTOR-dependent [92]. Also, phosphorylation of human MCM2 (only present in non-induced cells – **Table 2**) to Ser139, downstream of mTOR signaling [92], is pivotal in Cdc7/Dbf4-mediated phosphorylation of MCM2 in the initiation of DNA replication [102].

Together with other differential phosphorylation events mentioned above, since all of the observed differential phosphorylations present in the non-induced controls and absent in TAp73α-induced cells had already been reported to be dependent on mTOR-activation [92], we could conclude that TAp73α might trigger activation of specific phosphatases upstream of mTOR signaling. Since PI3K/Akt/mTOR signaling is important to interconnect cell growth with the regulation of the cellular metabolism, we decided to perform extensively metabolomics analyses and correlated it with proteomics results

3.2 METABOLOMICS ANALYSIS

Untargeted metabolomics results are plotted in **Figure 9**, as fold-change variations of metabolites upon induction of TAp73α expression, normalized to non-induced controls. Metabolites are grouped through a pathway-based criterion:

a) glycolysis (**Figure 9.A)**,

b) Krebs cycle (**Figure 9.B**),

c) glutathione (GSH) homeostasis (**Figure 9.C**),

d) Pentose Phosphate Pathway (PPP) (**Figure 9.D**),

e) purine metabolism and other signaling (**Figure 9.E**),

f) arginine-citrulline-NO metabolism (**Figure 9.F**).

Results were also plotted as a metabolic interaction network on the basis of whole metabolome maps from KEGG pathway.

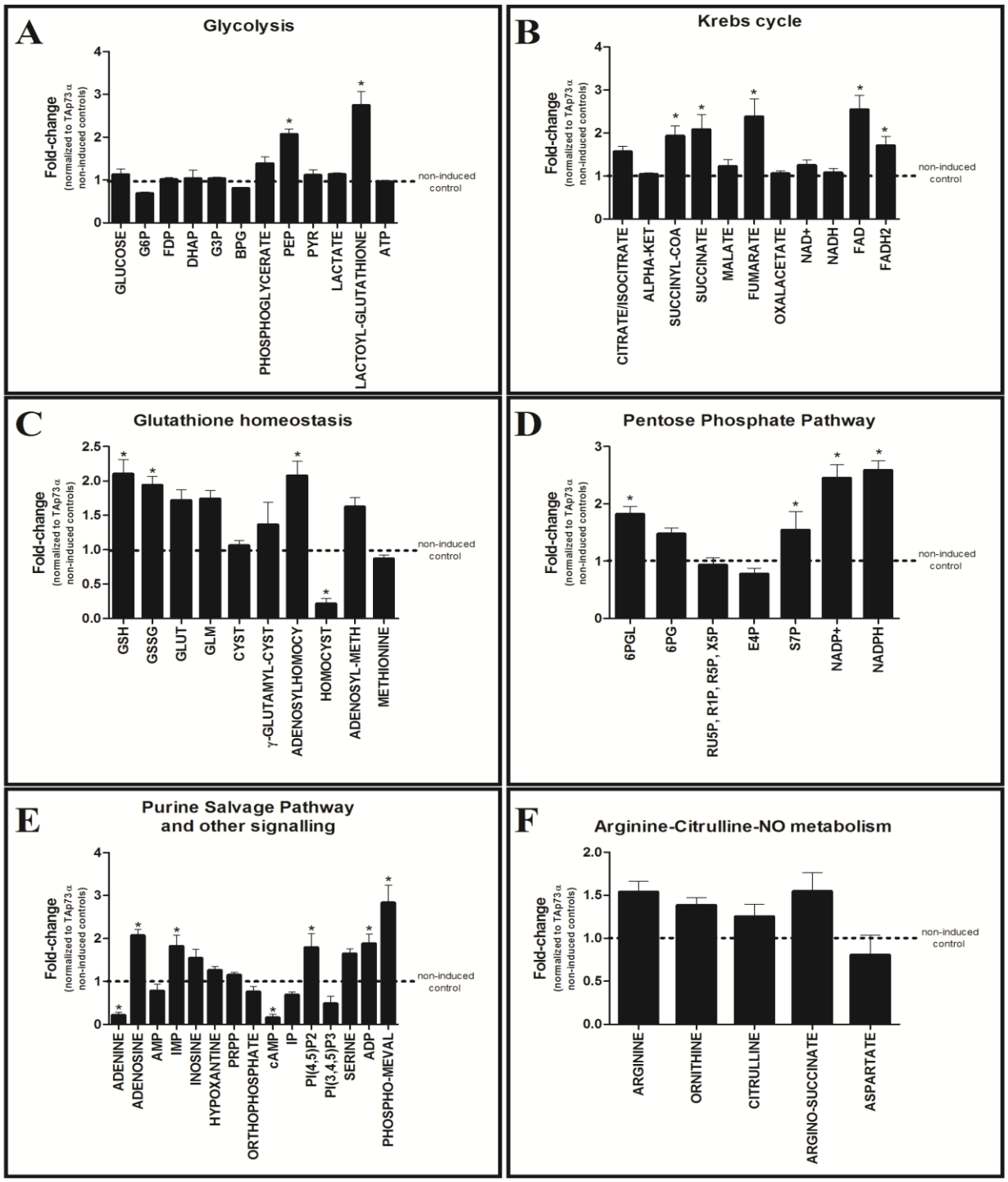

Figure 9 Pathway-wise plotting of untargeted metabolomics results, including glycolysis **(A)**, Krebs cycle **(B)**, GSH homeostasis **(C)**, pentose phosphate pathway **(D)**, purine metabolism and other signaling **(E)**, and arginine-citrulline-NO metabolism **(F)**. Results are plotted as mean of values detected for each metabolite in TAp73α-induced cells upon normalization to non-induced controls as means ± SEM. Asterisk indicate statistical significancy (p-value < 0.05 T-test of induced vs non-induced control values and fold-change ≥ |2|).

3.2.1 PIP2 and PIP3, IP3 and cAMP

On the basis of the assumption of a likely role of the PI3K/Akt/mTOR signaling in TAp73α-modulated events, we assayed the levels of phosphatidylinositol (3,4,5)-trisphosphate (PtdIns (3,4,5)P3 or PIP3) and biphosphate product PIP2 (PtdIns(4,5)P2) **(Figure 9.E)**.

Myo-inositol (1,4,5) triphosphate (IP3 – **Figure 9.E**) is a second messenger produced primarily in response to the stimulation of G-protein-coupled receptor or receptor tyrosine kinases. IP3 acts on the IP3 receptor (IP3R), an ER Ca^{2+} release channel which transmits Ca^{2+} spikes generated by the ER to mitochondria [103]. In particular, IP3-mediated Ca2+ signaling is critical for starvation-induced autophagy stimulation [103,104]. The increase of IP3 levels in TAp73α-induced cells (**Figure 9.E**) might stem from a crosstalk between pathways downstream to p73 activation either leading to apoptosis or autophagy through a delicate balance [104, 105].

We also observed decreases of the cAMP levels upon induction of the expression of TAp73α (**Figure 9.E**), an event that can be suggestive of a metabolic switch leading to demodulation of the cAMP-mediated activation of PKA, which is known to result in the inhibition of p73 protein activity [106].

3.2.2 Krebs cycle over-activation

It has been recently demonstrated that TAp73 yields the activation of mitochondrial metabolism, utterly resulting in ROS production and rerouting of cancer metabolic fluxes away from the so-called Warburg effect [107]. Accordingly, we found an over-activation of the Krebs cycle intemediates (citrate/isocitrate, succinyl-coA, succinate, malate, fumarate and FADH2) in TAp73α-induced SAOS-2 cells (**Figure 9.B**).

These metabolic changes were supported at the protein level by the TAp73α-dependent upregulation of the Krebs cycle enzyme mitochondrial dihydrolipoamide succinyltransferase (spot no. 494), ATP synthase subunit beta (spot no. 1454 and 1478 in Table 1),35 and prohibitin (spot no. 987, Table 1), a regulator of the mitochondrial respiration activity.[108]

Prohibitin expression is induced by metabolic stress caused by an imbalance in the synthesis of mitochondrial- and nuclear-encoded mitochondrial proteins [109]. Indirect evidences about mitochondrial transcription unbalance derive from the TAp73α-induced down-modulation of the

mitochondrial ribosomal protein L12 (spot n. 1231 and 1441 - **Table 1**), which is known to selectively associate with human mitochondrial RNA polymerase to activate transcription [110].

3.2.3 Glutathione homeostasis

In like fashion to p53 [111], TAp73 is able to drive the expression of glutaminase type 2 (GLS2), acting on specific p53 responsive elements present on its promoter (Velletri et al., submitted). GLS2 catalyzes the conversion of glutamine to glutamate and boosts GSH homeostasis by triggering accumulation of both reduced (GSH) and oxidized forms of glutathione (GSSG) [112, 113]. Since the levels of α-ketoglutarate did not substantially vary upon TAp73α expression (Figure 3B), we could assume that glutamine (i) might enter the Krebs cycle (which was indeed overactivated, previous paragraph) and (ii) might serve as a substrate for GSH metabolism. Consistently with these assumptions, we detected up-regulation of all the aforementioned metabolites (glutamine, glutamate, GSH and GSSG), and of other molecules indirectly involved in GSH metabolism as they promote cysteine biosynthesis (adenosyl-homocysteine and adenosyl-methionine) (**Figure 9.C**). In **Figure 10,** we provide a detail of the extracted ion chromatogram (EIC) for GSSG in TAp73α-induced and non-induced cells.

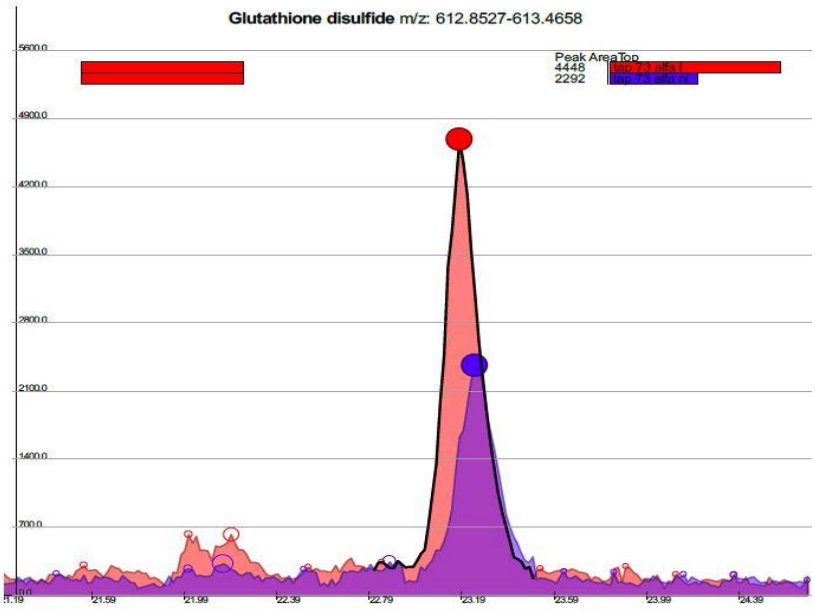

Figure 10. A detail of the extracted ion chromatogram (EIC) for GSSG in TAp73α-induced and non-induced cells.

3.2.4 Shift of glycolysis towards phosphoenolpyruvate accumulation and serine biosynthesis

While early glycolysis intermediates did not show any major fluctuations, we observed that TAp73 expression induces the accumulation of phosphoenolpyruvate (PEP – **Figure 9.A**). Conversion of phosphoenolpyruvate to pyruvate and generation of ATP by pyruvate kinase represents a rate-limiting step in glycolysis. Embryonic cells and tumor cells predominantly express a splicing variant of pyruvate kinase found in muscle, PKM2 [109]. PKM2 cells maintain higher flux to the serine synthetic pathway [110]. Indeed, glycolytic intermediates (especially phosphoglycerate and PEP) derived from enhanced glycolysis in cancer cells can be shunted to generate nonessential amino acids, such as serine [110]. In agreement, we detected higher levels of serine in TAp73 expressing cells (Purine metabolism and other signaling - **Figure 9.E**). Notably, PKM2 is reported amongst the p53/p63/p73 family targets in the p53FamTag database [111]. Enhanced mitochondrial activity described above resulted in the likely accumulation of ROS, as reflected by increased levels of lactoyl-glutathione (**Figure 9.A**) and alteration of GSH homeostasis.

3.2.5 Pentose Phosphate pathway

Reduction of GSSG to GSH to reload the antioxidant battery requires the reduced coenzyme NADPH. NADPH is largely produced from NADP+ through the PPP. However, NADPH also serves as a key coenzyme in anabolic pathways, including fatty acid biosynthesis, which is required for actively proliferating cells. In this view, p53 exerts its tumor suppressor activity also by depressing NADPH production through direct binding to and inhibition of the first and rate limiting enzyme of the PPP, glucose 6-phosphate dehydrogenase.96 Alternatively, p53 is known to boost the PPP via the up-regulation of TIGAR, which in turn results in a reduced flux through glycolysis and an increase in the rates of PPP.34 In the present study, TAp73α seems to promote PPP activity. Indeed, we found an accumulation of the oxidative phase intermediates of the PPP in TAp73α expressing cells (6- phosphogluconolactone, 6PGL; 6-phosphogluconic acid, 6PG; NADP+ and NADPH, Figure 3D).

Untargeted metabolomics revealed up-regulation of the whole PPP. In order to validate these results, we performed a targeted metabolomics approach through MRM analyses. In **Figure 11**,

we reported the MRM spectra for NADPH (**Figure 11.A -** upper row) and 6-phosphogluconic acid (**Figure 11.B** - lower row). At the protein level, expression of TAp73α resulted in the up-regulation of 6-phosphogluconolactonase (PGLS - spot no. 987 - **Table 1**), the PPP enzyme that converts 6-phosphogluconolactone to 6-phosphogluconate. This was not totally unexpected, since *in silico* prediction of p53/p63/p73 family-RE through p53FamTag [111-114] indicated the presence of two REs in the promoter region of the PGLS gene, suggesting a potential transcriptional regulation of this enzyme by TAp73. To confirm this assumption, we measured PGLS mRNA levels in control and in TAp73α expressing cells by qRT-PCR and we found that PGLS2 transcript levels are indeed increased in TAp73α-induced cells (**Figure 12**).

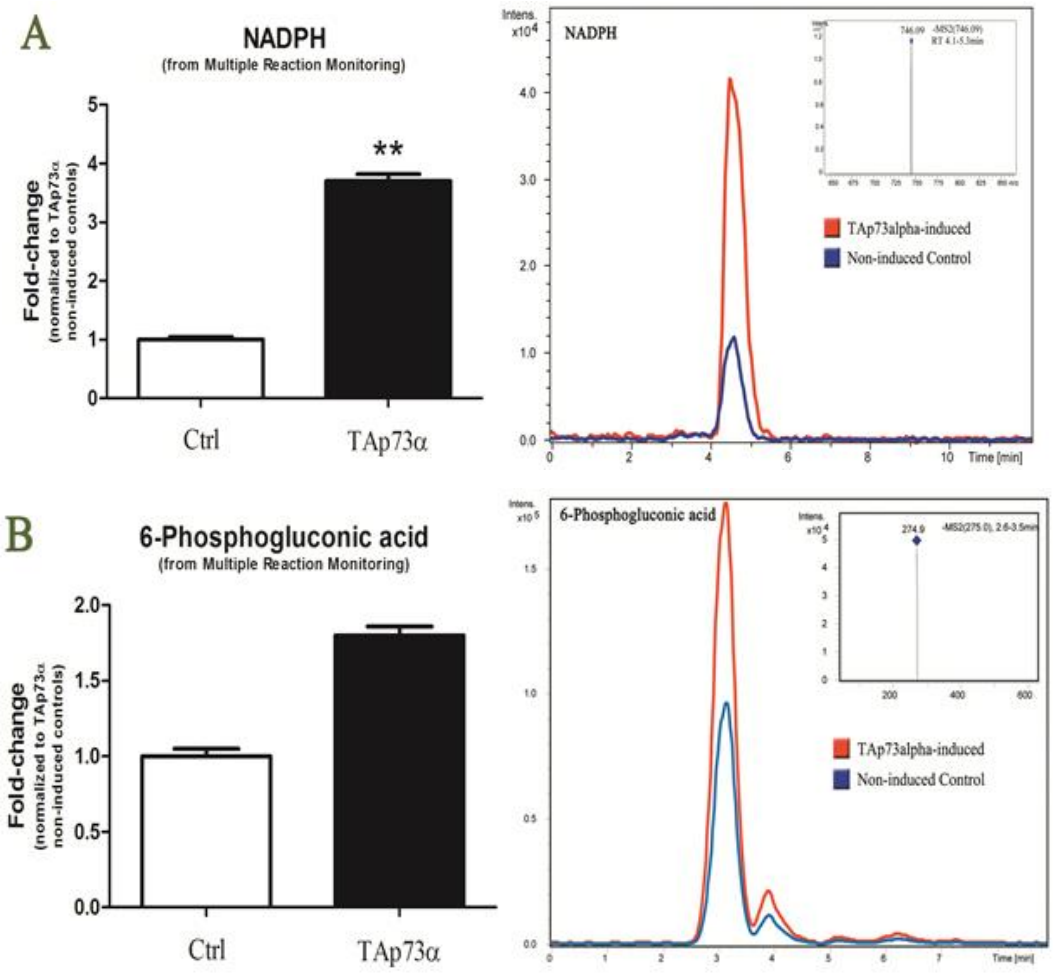

Figure 11 A detail of the results from Multiple Reaction Monitoring (MRM) analyses of NADPH **(A)** and 6-phosphogluconic acid **(B)**. Graphpad results are plotted as fold change variation in TAp73α-induced SAOS-2 cells normalized to non-induced controls. In the right panel, a detail of the extracted ion chromatograms (EIC) for the selected metabolites.

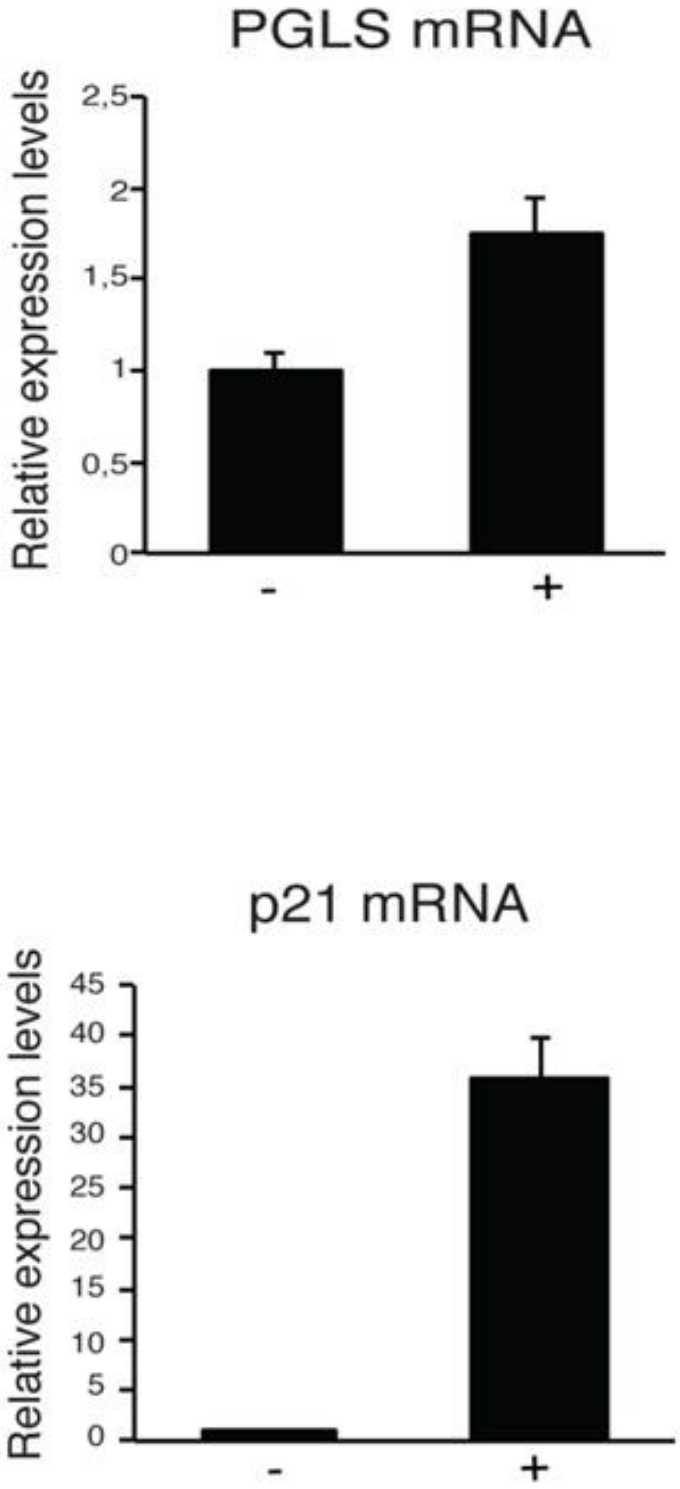

Figure 12 SAOS-2-TAp73α were treated with doxycyclin (2 μg/ml) for twenty-four hours and total RNA was extracted and utilized for reverse transcription and quantitative real-time PCR (qRT-PCR) using specific primers for human PGLS2, p21 and β Actin (for quantity normalization). Results are shown as mean ± SD of three independent experiments.

3.2.6 Purine metabolism

With respect to purine metabolism, TAp73α shows opposite transcriptional behavior in comparison to p53 and the TAp73β isoform. Indeed, while p53 and p73β down-regulate the expression of adenosine deaminase (ADA),76 TAp73α promotes ADA expression,[115] although ADA protein levels might not proportionally increase (spot no. 649, Table 1). The ADA enzyme is involved in nucleotide metabolism, the deficit of which causes the inhibition of DNA synthesis and repair. ADA irreversibly deaminates adenosine, converting it to the related nucleoside inosine by the substitution of the amino group for a hydroxyl group. Consistently, we found an increase of both inosine and adenosine upon induction of TAp73α expression **(Figure 3E)**.

3.2.7 Arginine-citrulline-NO metabolism

Nitric oxide (NO) is synthesized from arginine and O2 by NO synthase (NOS). Citrulline formed as a byproduct of the NOS reaction can be recycled to arginine by argininosuccinate synthetase (AS) and argininosuccinate lyase (AL). AS and sometimes AL are coinduced with inducible NOS (iNOS) in several cell lines,98 whereby NO was synthesized from citrulline (via arginine) as well as from arginine, indicating the activation of the citrulline− NO cycle [116]. As a result, high concentrations of NO (and NOderived reactive nitrogen species, RNS) induce apoptosis by activating the p53-dependent pathway (and possibly the p73- dependent pathway), while lower concentrations of NO induce apoptosis by ER stress [116]. In the present study, we found accumulation of all the metabolites involved in the arginine− citrulline−NOmetabolism (arginine, argino succinate, citrulline, ornithine, **Figure 9 F**).

3.3 LIPIDOMICS

Finally, we investigated the TAp73α-mediated modulation of intracellular lipid content by analyzing the lipidic fraction of metabolic extracts and performing targeted MRM analyses on a shortlist of selected lipids. The accumulation of NADPH observed in the TAp73α expressing cells should result in the accumulation of long chain fatty acids, in the light also of the evidence that p53/p63/p73 family members induce the expression of fatty acid synthase (FASN), a key enzyme involved in the biogenesis of membrane lipids [117]. In particular, the ectopic expression of TAp73alpha and ΔNp63alpha leads to an increase of FASN mRNA levels [118]. Confirmatory hints were obtained from untargeted metabolomics when biosynthetic pathways for long chain saturated and unsaturated fatty acids were considered (**Figures 13 and 14**).

Through the analysis of the lipidic fraction of metabolic extracts, we confirmed the presence of higher levels of long chain fatty acids in TAp73α-induced cells in comparison to non-induced cells (**Figure 13**).

At the protein level, we found that TAp73α induction is paralleled by a decrease of enoyl-CoA hydratase (spot no. 998, Table 1). This enzyme is involved in the beta-oxidation pathway,[119] by hydrating the double bond between the second and third carbons on acyl-CoA.

Taken together, these results indicate that the expression of TAp73α might influence lipid biosynthesis and lipid oxidation to a certain extent in the absence of external stimuli. For example, we showed the differential expressions of the polyunsaturated 7,10,13,16-docosatetraenoic acid, a polyunsaturated fatty acid that acts as a potent apoptotic inducer[120]. Likewise, differential expression of ceramide 22:0 (**Figure 13**) upon expression of TAp73α might be suggestive of increased lipid-mediated growth arrest and apoptosis signaling.[121-124]

Furthermore, the concept about the role of lipid oxidation (especially of gamma-linolenic acid, arachidonic acid, eicosapentaenoic acid and decosahexaenoic acid) in the promotion of cell death through a mechanism mediated by the cytochrome p450, cyclooxygenase (COX) and lipoxygenase (LOX)-dependent oxidation of long-chain fatty acids to prostaglandins, thromboxanes and leukotrienes. In order to test this hypothesis, we investigated the accumulation of these oxidized lipid species and reported the TAp73α-dependent accumulation of prostaglandins (B1, D3/E3, F1α), leukotrienes (A4, B4, C4, D4, F4) and some oxy-sterols (cholest-5-ene-3β,26-diol) (**Figure 14).**

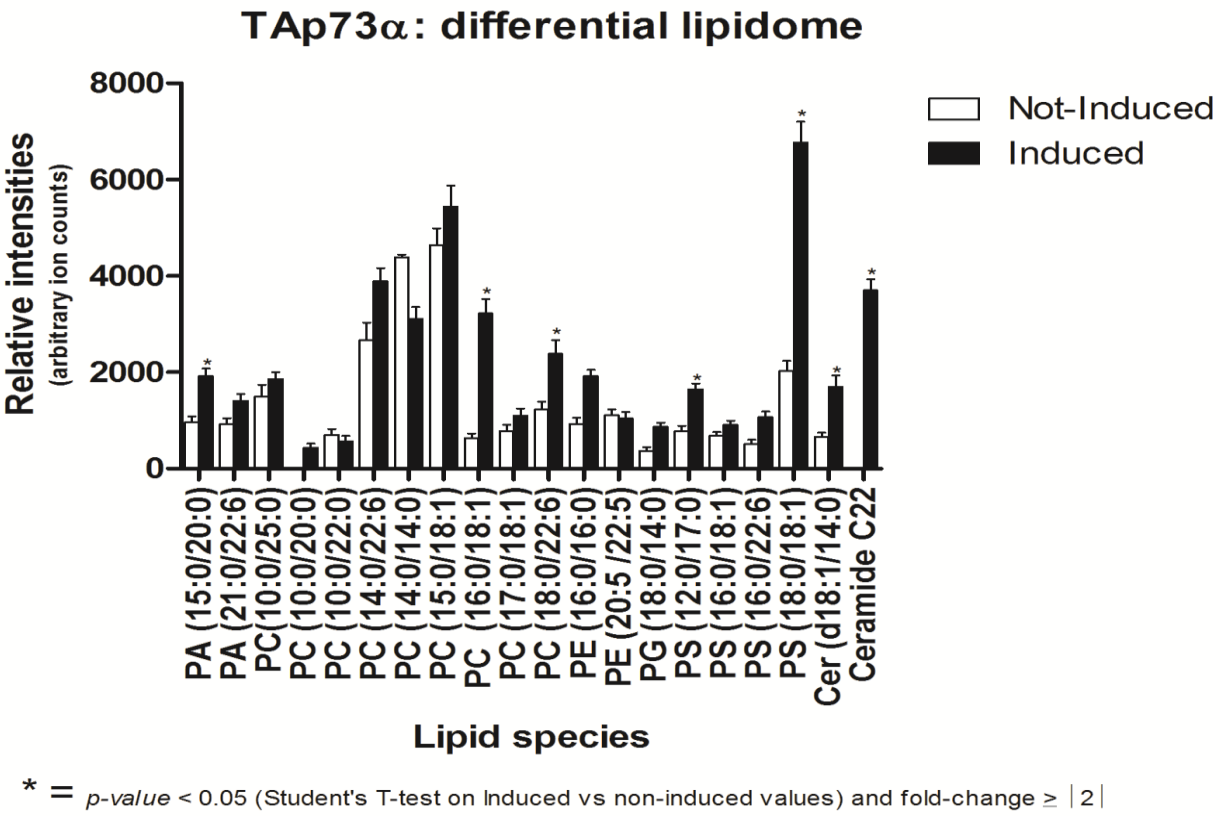

Figure 13 Results from Multiple Reaction Monitoring (MRM) analyses of a shortlist of selected lipids. Graphpad results are plotted as fold change variation in TAp73α-induced SAOS-2 cells normalized to non-induced controls. *Asterisk indicate statistical significancy (p-value < 0.05 T-test of induced vs non-induced control values and fold-change* $\geq |2|$*).*

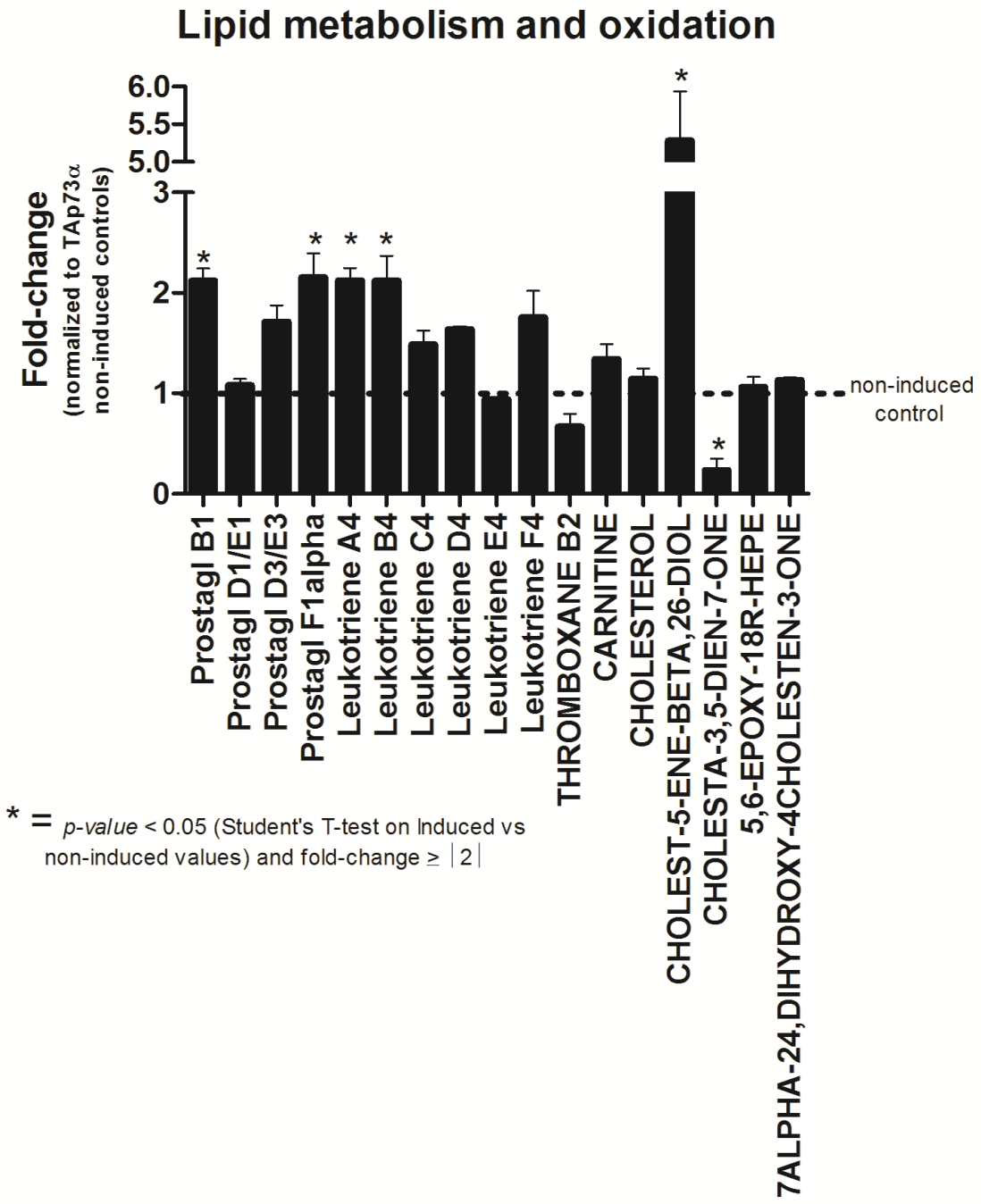

Figure 14 Results from Multiple Reaction Monitoring (MRM) analyses of the main products of lipid peroxidation from untargeted metabolomics. Graphpad results are plotted as fold change variation in TAp73α-induced SAOS-2 cells normalized to non-induced controls. *Asterisk indicate statistical significancy (p-value < 0.05 T-test of induced vs non-induced control values and fold-change ≥ |2|).*

4 CONCLUSION

The simultaneous application of multiple omics approaches helped us to collect enough pieces from the jigsaw puzzle of TAp73α downstream activated pathways to allow us to suggest biological interpretations, which will deserve further ad hoc investigations to collect the missing pieces through targeted approaches in the near future. From the present study, a role emerged for TAp73α at the crossroads between prosurvival autophagic signals and ER stress/mitochondrial proapoptotic pathways. Biologically, these opposite signals balance each other resulting in cell cycle arrest within 24 h from the induction of TAp73α.

Several lines of evidence underpin this statement, both at the protein and at the metabolic level, which integrate complementary evidence already available from the literature.

First of all, expression of TAp73α in SAOS-2 cells results in the stabilization, accumulation, and promotion of p73 activity through up-regulation of the interacting partners HSP90 and 14-3-3ε. TAp73α expression also promotes the activation of transcription (RNA pol II), mRNA splicing (serine/arginine-rich splicing factor 1 isoform 1), and translation (eIF-3 complex). Evidences about TAp73α-provoked ER-stress (previously documented with the involvement of Scotin [11]), were hereby indirectly supported by alterations to protein folding (PDIA5) and might involve RAD23 protein, which takes part in DNA-damage repairing and ER stress. ER-stress was indirectly related at the metabolic level to ER (and mitochondrial) Ca^{2+} release, which is known to occur in response to IP3 accumulation (hereby observed upon expression of TAp73α). Moreover, shift of glycolysis towards PEP accumulation and serine biosynthesis is consistent with the activation of the autophagic signaling.

Despite sharing several features with other components of thep53 family in terms of downstream effectors, TAp73α favored purine metabolism through the up-regulation of ADA synthesis and accumulation of purine metabolites. This results in survival signaling, analogously to what has been recently reported for p53 in the absence of external stimuli [34].

At the metabolic level, TAp73α-dependent induction of oxidative stress is documented by several indicators, including the accumulation of lactoyl-glutathione, the alteration of GSH homeostasis (related to induction of GLS2 expression), and lipid peroxidation. In this view, up-modulation of the arginine−citrulline−NO metabolism might end up producing NO and promoting low RNS stress, which in turn would trigger ER stress or high RNS, thereby favoring DNA damage and apoptosis. PPP overactivation (as gleaned from the TAp73α-dependent

upregulation of 6-phosphogluconolactonase) promoted NADPH production as a reducing coenzyme for antioxidant cascades but also for lipid biosynthesis.

Expression of TAp73α in SAOS-2 cells was also accompanied by increased rates of Krebs metabolism (citrate/isocitrate, succinyl-coA, succinate, malate, fumarate, and FADH2 were detected in TAp73α-induced SAOS-2 cells) and Krebs-related proteins (ATP synthase subunit beta, mitochondrial precursor, and prohibitin), which is consistent with previous reports about TAp73α mediating ROS production through mitochondrial activation and mitochondrial intrinsic apoptotic pathways. In particular, the protein prohibitin is also tied to an imbalance in the synthesis of mitochondrial- and nuclear-encoded mitochondrial proteins, further supported by TAp73α-mediated downregulation of mitochondrial ribosomal protein L12.

TAp73α also interfered with the fine tuning of lipid synthesis and oxidative metabolism, which is supported by either TAp73α-dependent up-regulation of FASN in the literature and hereby by the opposite modulation of the expression of delta2-enoyl-CoA isomerase and enoyl-CoA hydratase in TAp73α-induced in relation to non-induced cells. Lipid metabolism was hereby driven towards the accumulation and oxidation of the long-chain fatty acids with pro-apoptotic potential (polyunsaturated 7,10,13,16-docosatetraenoic acid and ceramide 22).

Cyclic AMP decreased upon expression of TAp73α, which should in turn reduce the activation of PKA, whose kinase activity inhibits p73.

Regarding the phosphoproteomics analysis, we found dephosphorylation of several proteins (proteasome subunit alpha type-3, MAP4, GOK, EIF1D, MCM2) associated with spindle checkpoint and mitosis in non-induced cells. It is worth noting that phosphorylation of these proteins is regulated by the PTEN pathway,[124,125] suggesting a potential role of TAp73α in regulating this pathway. PTEN contribution in TAp73α-mediated cascades should result in the inhibition of PI3K, hereby indirectly assessed through the increase in the levels of PIP2 and decrease of PIP3, which is known to result in the inhibition of Akt and promotion of apoptosis in SAOS-2 cells.

In conclusion, the simultaneous application of multiple omics approaches helped us to draw a global picture of the TAp73α downstream activated pathways, which paves the way to further our understanding the role of p73 either in mediating cell survival or promoting tumor suppression signaling.

References

1. Kaghad, M. et al. Monoallelically expressed gene related to p53 at 1p36, a region frequently deleted in neuroblastoma and other human cancers. Cell 1997; 90:809–819
2. Murray-Zmijewski F, Lane DP, Bourdon JC. p53/p63/p73 isoforms: an orchestra of isoforms to harmonise cell differentiation and response to stress. Cell Death Differ. 2006;13(6):962-72.
3. Collavin L, Lunardi A, Del Sal G. p53-family proteins and their regulators: hubs and spokes in tumor suppression. Cell Death Differ. 2010;17(6):901-11
4. De Laurenzi V, Costanzo A, Barcaroli D, Terrinoni A, Falco M, Annicchiarico-Petruzzelli M, Levrero M, Melino G. Two new p73 splice variants, gamma and delta, with different transcriptional activity. J Exp Med. 1998;188(9):1763-8.
5. Laurenzi VD, Catani MV, Terrinoni A, Corazzari M, Melino G, Costanzo A, Levrero M, Knight RA. Additional complexity in p73: induction by mitogens in lymphoid cells and identification of two new splicing variants epsilon and zeta. Cell Death Differ 1999;6(5):389-90.
6. Ramadan S, Terrinoni A, Catani MV, Sayan AE, Knight RA, Mueller M, Krammer PH, Melino G, Candi E. p73 induces apoptosis by different mechanisms. Biochem Biophys Res Commun. 2005;331(3):713-7.
7. Rossi M, Sayan AE, Terrinoni A, Melino G, Knight RA. Mechanism of induction of apoptosis by p73 and its relevance to neuroblastoma biology. Ann N Y Acad Sci. 2004;1028:143-9.
8. Toh WH, Nam SY, Sabapathy K. An essential role for p73 in regulating mitotic cell death. Cell Death Differ. 2010;17(5):787-800
9. Fricker M, Papadia S, Hardingham GE, Tolkovsky AM. Implication of TAp73 in the p53-independent pathway of Puma induction and Puma-dependent apoptosis in primary cortical neurons. J Neurochem 2010;114(3):772-83.
10. Martin AG, Trama J, Crighton D, Ryan KM, Fearnhead HO. Activation of p73 and induction of Noxa by DNA damage requires NF-kappa B. Aging (Albany NY). 20091(3):335-49.
11. Terrinoni A, Ranalli M, Cadot B, Leta A, Bagetta G, Vousden KH, Melino G. p73-alpha is capable of inducing scotin and ER stress. Oncogene. 2004;23(20):3721-5.
12. Melino G, Lu X, Gasco M, Crook T, Knight RA. Functional regulation of p73 and p63: development and cancer. Trends Biochem Sci. 2003;28(12):663-70.

13. Conforti F, Sayan AE, Sreekumar R, Sayan BS. Regulation of p73 activity by post-translational modifications. Cell Death Dis. 2012 Mar 15;3:e285. doi: 10.1038/cddis.2012.2
14. Urist M, Tanaka T, Poyurovsky MV, Prives C. p73 induction after DNA damage is regulated by checkpoint kinases Chk1 and Chk2. Genes Dev. 2004;18(24):3041-54.
15. Lee YG, Lee SW, Sin HS, Kim EJ, Um SJ. Kinase activity-independent suppression of p73alpha by AMP-activated kinase alpha (AMPKalpha). Oncogene. 2009;28(7):1040-52.
16. Gong JG, Costanzo A, Yang HQ, Melino G, Kaelin WG Jr, Levrero M, Wang JY. The tyrosine kinase c-Abl regulates p73 in apoptotic response to cisplatin-induced DNA damage. Nature. 1999;399(6738):806-9.
17. Agami R, Blandino G, Oren M, Shaul Y. Interaction of c-Abl and p73alpha and their collaboration to induce apoptosis. Nature. 1999; 399(6738):809-13.
18. Melino G, De Laurenzi V, Vousden KH. p73: friend or foe in tumorigenesis. Nat Rev Cancer 2002; 2: 605–615.
19. Stiewe T, Pützer BM. Role of p73 in malignancy: tumor suppressor or oncogene? Cell Death Differ. 2002;9(3):237-45.
20. Bailey SG, Cragg MS, Townsend PA. Family friction as ΔNp73 antagonises p73 and p53. Int J Biochem Cell Biol. 2011;43(4):482-6.
21. Killick R, Niklison-Chirou M, Tomasini R, Bano D, Rufini A, Grespi F, Velletri T, Tucci P, Sayan BS, Conforti F, Gallagher E, Nicotera P, Mak TW, Melino G, Knight RA, Agostini M. p73: a multifunctional protein in neurobiology. Mol Neurobiol. 2011;43(2):139-46.
22. Horvilleur E, Bauer M, Goldschneider D, Mergui X, de la Motte A, Bénard J, Douc-Rasy S, Cappellen D. p73alpha isoforms drive opposite transcriptional and post-transcriptional regulation of MYCN expression in neuroblastoma cells. Nucleic Acids Res. 2008;36(13):4222-32.
23. Conforti F, Yang AL, Agostini M, Rufini A, Tucci P, Nicklison-Chirou MV, Grespi F, Velletri T, Knight RA, Melino G, Sayan BS. Relative expression of TAp73 and ΔNp73 isoforms. Aging (Albany NY). 2012;4(3):202-5.
24. Tebbi A, Guittet O, Cottet MH, Vesin MF, Lepoivre M. TAp73 induction by nitric oxide: regulation by checkpoint kinase 1 (CHK1) and protection against apoptosis. J Biol Chem. 2011;286(10):7873-84.
25. Nyman U, Muppani NR, Zhivotovsky B, Joseph B. Hsp72 mediates TAp73α anti-apoptotic effects in small cell lung carcinoma cells. J Cell Mol Med 2011;15(8):1757-68.

26. Muppani N, Nyman U, Joseph B. TAp73alpha protects small cell lung carcinoma cells from caspase-2 induced mitochondrial mediated apoptotic cell death. Oncotarget. 2011;2(12):1145-54.
27. Vikhanskaya F, D'Incalci M, Broggini M. p73 competes with p53 and attenuates its response in a human ovarian cancer cell line. Nucleic Acids Res. 2000;28(2):513-9.
28. Boominathan L. The guardians of the genome (p53, TA-p73, and TA-p63) are regulators of tumor suppressor miRNAs network. Cancer Metastasis Rev 2010;29(4):613-39.
29. Knouf EC, Garg K, Arroyo JD, Correa Y, Sarkar D, Parkin RK, Wurz K, O'Briant KC, Godwin AK, Urban ND, Ruzzo WL, Gentleman R, Drescher CW, Swisher EM, Tewari M. An integrative genomic approach identifies p73 and p63 as activators of miR-200 microRNA family transcription. Nucleic Acids Res. 2012;40(2):499-510.
30. Chen B, Li H, Zeng X, Yang P, Liu X, Zhao X, Liang S. Roles of microRNA on cancer cell metabolism. J Transl Med. 2012;10(1):228.
31. Peschiaroli A, Giacobbe A, Formosa A, Markert EK, Bongiorno-Borbone L, Levine AJ, Candi E, D'Alessandro A, Zolla L, Finazzi Agrò A, Melino G. miR-143 regulates hexokinase 2 expression in cancer cells. Oncogene. 2012. doi:10.1038/onc.2012.100.
32. Hanahan D, Weinberg RA. Hallmarks of cancer: the next generation. Cell. 2011;144(5):646-74.
33. Markert EK, Levine AJ, Vazquez A. Proliferation and tissue remodeling in cancer: the hallmarks revisited. Cell Death Dis. 2012;3:e397
34. Cheung EC, Vousden KH. The role of p53 in glucose metabolism. Curr Opin Cell Biol. 2010;22(2):186-91.
35. Rufini A, Niklison-Chirou MV, Inoue S, Tomasini R, Harris IS, Marino A, Federici M, Dinsdale D, Knight RA, Melino G, Mak TW. TAp73 depletion accelerates aging through metabolic dysregulation. Genes Dev. 2012;26(18):2009-14.
36. J. Petrak, R. Ivanek, O. Toman, R. Cmejla, J. Cmejlova, D. Vyoral et al. Déjà vu in proteomics A hit parade of repeatedly identified differentially expressed proteins Proteomics 2008; 8:1744–9.
37. S. Rogers, M. Girolami, W. Kolch, K.M. Waters, T. Liu, B. Thrall et al. Investigating the correspondence between transcriptomic and proteomic expression profiles using coupled cluster models Bioinformatics 2008; 24(24) 2894–900.
38. D'Alessandro A, Zolla L. Meat science: From proteomics to integrated omics towards system biology. J Proteomics. 2012. doi:pii: S1874-3919(12)00718-X.

39. Lane, D.P. and Crawford, L.V. (1979) T antigen is bound to a host protein in SV40-transformed cells. Nature 278, 261–263
40. E. T. Wang, R. Sandberg, S. Luo et al., "Alternative isoform regulation in human tissue transcriptomes," *Nature*, vol. 456, no. 7221, pp. 470–476, 2008.
41. Q. Pan, Q. Shai, L. J. Lee, B. J. Frey, and B. J. Blencowe, "Deep surveying of alternative splicing complexity in the human transcriptome by high-throughput sequencing," *Nature Genetics*, vol. 40, no. 12, pp. 1413–1415, 2008.
42. Mills AA, Zheng B, Wang XJ, Vogel H, Roop DR, Bradley A. p63 is a p53 homologue required for limb and epidermal morphogenesis. Nature 1999; 398: 708–713.
43. Mills AA, Zheng B, Wang XJ, Vogel H, Roop DR, Bradley A. p63 is a p53 homologue required for limb and epidermal morphogenesis. Nature 1999; 398: 708–713.
44. Yang A, Schweitzer R, Sun D, Kaghad M, Walker N, Bronson RT et al. p63 is essential for regenerative proliferation in limb, craniofacial and epithelial development. Nature 1999; 398: 714–718.
45. J. C. Bourdon, K. Fernandes, F.Murray-Zmijewski et al., "p53 isoforms can regulate p53 transcriptional activity," *Genes and Development*, vol. 19, no. 18, pp. 2122–2137, 2005.].
46. V. Dötsch, F. Bernassola, D. Coutandin, E. Candi, and G. Melino, "p63 and p73, the ancestors of p53," Cold Spring Harbor perspectives in biology, vol. 2, no. 9, p. a004887, 2010.
47. R. Rutkowski, K. Hofmann, and A. Gartner, "Phylogeny and function of the invertebrate p53 superfamily," Cold Spring Harbor Perspectives in Biology, vol. 2, no. 7, Article ID a001131, 2010.
48. Flaman J-M, Waridel F, Estreicher A, Vannier A, Limacher J-M, Gilbert D, Iggo R and Frebourg T (1996) The human tumor suppressor gene p53 is alternatively spliced in normal cells. Oncogene 12: 813–818.
49. Hofstetter G, Berger A, Fiegl H, Slade N, Zori A, Holzer B, Schuster E, Mobus V J, Reimer et al. 2010 Alternative splicing of p53 and p73: the novel p53 splice variant p53delta is an independent prognostic marker in ovarian cancer. *Oncogene 29*: 1997–2004
50. 18. Osada M, Park HL, Nagakawa Y, Yamashita K, Fomenkov A, Kim MS, Wu G, Nomoto S, Trink B and Sidransky D (2005) Differential recognition of response elements determines target gene specificity for p53 and p63. Mol. Cell. Biol. 25: 6077–6089.
51. Benard J, Douc-Rasy S and Ahomadegbe JC (2003) TP53 family members and human cancers. Hum. Mutat. 21: 182–191.

52. Dohn M, Zhang S and Chen X (2001) p63alpha and DeltaNp63alpha can induce cell cycle arrest and apoptosis and differentially regulate p53 target genes. Oncogene 20: 3193–3205.
53. Wu G, Nomoto S, Hoque MO, Dracheva T, Osada M, Lee CC, Dong SM, Guo Z, Benoit N, Cohen Y, Rechthand P, Califano J, Moon CS, Ratovitski E, Jen J, Sidransky D and Trink B (2003) DeltaNp63alpha and TAp63alpha regulate transcription of genes with distinct biological functions in cancer and development. Cancer Res. 63: 2351–2357.
54. Melino G, De Laurenzi V, Vousden KH. 2002. p73: Friend or foe in tumorigenesis. Nat Rev Cancer 2: 605–615.
55. Melino G, Lu X, Gasco M, Crook T, Knight RA. 2003. Functional regulation of p73 and p63: development and cancer. Trends Biochem Sci 28: 663–670.
56. Yang A, Walker N, Bronson R, Kaghad M, Oosterwegel M, Bonnin J, Vagner C, Bonnet H, Dikkes P, Sharpe A, et al. 2000. P73-deficient mice have neurological, pheromonal and inflammatory defects but lack spontaneous tumours. Nature 404: 99–103.
57. McKeon F (2004) p63 and the epithelial stem cell: more than status quo? Genes Dev. 18: 465–469.
58. Koster MI, Kim S, Mills AA, DeMayo FJ and Roop DR (2004) p63 is the molecular switch for initiation of an epithelial stratification program. Genes Dev. 18: 126–131
59. Mills AA, Zheng B, Wang XJ, Vogel H, Roop DR and Bradley A (1999) p63 is a p53 homologue required for limb and epidermal morphogenesis (in Process Citation). Nature 398: 708–713.
60. Celli J, Duijf P, Hamel BC, Bamshad M, Kramer B, Smits AP, Newbury-Ecob R, Hennekam RC, Van Buggenhout G, van Haeringen A, Woods CG, van Essen AJ, de Waal R, Vriend G, Haber DA, Yang A, McKeon F, Brunner HG and van Bokhoven H (1999) Heterozygous germline mutations in the p53 homolog p63 are the cause of EEC syndrome. Cell 99: 143–153.
61. V. Dötsch, F. Bernassola, D. Coutandin, E. Candi and G. Melino p63 and p73, the Ancestors of p53 19, 2010 Cold Spring Harb Perspect Biol 2010; doi: 10.1101/cshperspect.a004887 originally published online May 24, 2014
62. Pozniak CD, Radinovic S, Yang A, McKeon F, Kaplan DR, Miller FD. 2000. An anti-apoptotic role for the p53 family member, p73, during developmental neuron death. Science 289: 304–306.

63. Jacobs WB, Govoni G, Ho D, Atwal JK, Barnabe-Heider F, Keyes WM, Mills AA, Miller FD, Kaplan DR. 2005. P63 is an essential proapoptotic protein during neural development. Neuron 48: 743–756.
64. D'Alessandro A, Gevi F, Zolla L. A robust high resolution reversed-phase HPLC strategy to investigate various metabolic species in different biological models. Mol Biosyst. 2011;7(4):1024-32.
65. Ivanova P.T. Milne S. B., Brown H.A. Identification of atypical ether-linked glyceriphospholipid species in macrophages by mass spectrometry. J. Lipid Res.51 (20010) 1581-1590.
66. Melamud E, Vastag L, Rabinowitz JD. Metabolomic analysis and visualization engine for LC-MS data. Anal Chem. 2010;82(23):9818-26.
67. Kanehisa M, Goto S. KEGG: kyoto encyclopedia of genes and genomes. Nucleic Acids Res. 2000; 28(1):27-30.
68. Mastro R, Hall M. Protein delipidation and precipitation by Tri-n-butylphosphate, Aceton and Methanol treatment for isoelesctric focusing and two-dimensional gel electrophoresis. Anal Biochem.1999;273(2):313-315.
69. Candiano G, Bruschi M, Musante L, Santucci L, Ghiggeri GM, Carnemolla B, Orecchia P, Zardi L, Righetti PG. Blue silver: a very sensitive colloidal Coomassie G-250 staining for proteome analysis. Electrophoresis. 2004 May;25(9):1327-33.
70. Shevchenko A, Wilm M, Vorm O, Mann M. Mass spectrometric sequencing of proteins silver-stained polyacrylamide gels. Anal Chem 1996;68:850–8.
71. Baker MA, Smith ND, Hetherington L, Pelzing M, Condina MR, Aitken RJ. Use of titanium dioxide to find phosphopeptide and total protein changes during epididymal sperm maturation. J Proteome Res 2011;10:1004–17.
72. Larsen MR, Thingholm TE, Jensen ON, Roepstorff P, Jorgensen TJ. Highly selective enrichment of phosphorylated peptides from peptide mixtures using titanium dioxide microcolumns. Mol Cell Proteomics 2005;4:873–86.
73. Hartmer R, Kaplan DA, Gebhardt CR, Ledertheil T, Brekenfeld A. Multiple ion/ion reactions in the 3D ion trap: selective reagent anion production for ETD and PTR from a single compound. Int J Mass Spectrom 2008;276:82–90.
74. Wang YT, Tsai CF, Hong TC, Tsou CC, Lin PY, Pan SH, et al. An informatics-assisted label-free quantitation strategy that depicts phosphoproteomic profiles in lung cancer cell invasion. J Proteome Res 2010;9:5582–97.

75. Wang C, Chen J. Phosphorylation and hsp90 binding mediate heat shock stabilization of p53. J Biol Chem. 2003;278(3):2066-71.
76. De Laurenzi V, et al. p63 and p73 transactivate differentiation gene promoters in human keratinocytes. Biochem Biophys Res Commun 2000;273(1):342–6.
77. Waterman MJ, et al. ATM-dependent activation of p53 involves dephosphorylation and association with 14-3-3 proteins. Nat Genet 1998;19(2):175–8.
78. Melino G, et al. Functional regulation of p73 and p63: development and cancer. Trends Biochem Sci 2003;28(12):663–70.
79. Hershko, A. and Ciechanover, A. The ubiquitin system. Annu Rev Biochem. 1998; 67: 425–479.
80. Bernassola F, Salomoni P, Oberst A, Di Como CJ, Pagano M, Melino G, Pandolfi PP. Ubiquitin-dependent degradation of p73 is inhibited by PML. J Exp Med. 2004;199(11):1545-57.
81. Pinton P, Giorgi C, Pandolfi PP. The role of PML in the control of apoptotic cell fate: a new key player at ER-mitochondria sites. Cell Death Differ. 2011;18(9):1450-6.
82. Asher, G., Tsvetkov, P., Kahana, C. and Shaul, Y. A mechanism of ubiquitin-independent proteasomal degradation of the tumour suppressors p53 and p73. Genes Dev 2005;19:316-21.
83. Salomoni P, Dvorkina M, Michod D. Role of the promyelocytic leukaemia protein in cell death regulation. Cell Death Dis. 2012 Jan 12;3:e247.
84. Balint, E., S. Bates, and K.H. Vousden. Mdm2 binds p73alpha without targeting degradation. Oncogene 1999; 18:3923–3929.
85. de Bie P, Ciechanover A. Ubiquitination of E3 ligases: self-regulation of the ubiquitin system via proteolytic and non-proteolytic mechanisms. Cell Death Differ. 2011;18(9):1393-402.
86. Satoh T, Ishizuka T, Tomaru T, Yoshino S, Nakajima Y, Hashimoto K, Shibusawa N, Monden T, Yamada M, Mori M. Tat-binding protein-1 (TBP-1), an ATPase of 19S regulatory particles of the 26S proteasome, enhances androgen receptor function in cooperation with TBP-1-interacting protein/Hop2. Endocrinology. 2009;150(7):3283-90.
87. Chen X, Yin XM. Coordination of autophagy and the proteasome in resolving endoplasmic reticulum stress. Vet Pathol. 2011;48(1):245-53.
88. Raciti M, Lotti LV, Valia S, Pulcinelli FM, Di Renzo L. JNK2 is activated during ER stress and promotes cell survival. Cell Death Dis. 2012 Nov 22;3:e429.

89. Civelek M, Manduchi E, Riley RJ, Stoeckert CJ Jr, Davies PF. Chronic endoplasmic reticulum stress activates unfolded protein response in arterial endothelium in regions of susceptibility to atherosclerosis. Circ Res. 2009;105(5):453-61.
90. van Laar T, van der Eb AJ, Terleth C. A role for Rad23 proteins in 26S proteasome-dependent protein degradation? Mutat Res. 2002;499(1):53-61.
91. Ohsawa S, Watanabe T, Katada T, Nishina H, Miura M. Novel antibody to human BASP1 labels apoptotic cells post-caspase activation. Biochem Biophys Res Commun. 2008;371(4):639-43.
92. Jost CA, Marin MC, Kaelin WG Jr. p73 is a simian [correction of human] p53-related protein that can induce apoptosis. Nature. 1997; 389(6647):191-4.
93. Schuler M, Bossy-Wetzel E, Goldstein JC, Fitzgerald P, Green DR. p53 induces apoptosis by caspase activation through mitochondrial cytochrome c release. J Biol Chem. 2000;275(10):7337-42.
94. Olsen JV, Vermeulen M, Santamaria A, Kumar C, Miller ML, Jensen LJ, Gnad F, Cox J, Jensen TS, Nigg EA, Brunak S, Mann M. Quantitative phosphoproteomics reveals widespread full phosphorylation site occupancy during mitosis. Sci Signal. 2010;3(104):ra3.
95. Rosenbluth JM, Pietenpol JA. mTOR regulates autophagy-associated genes downstream of p73. Autophagy. 2009;5(1):114-6.
96. Rosenbluth JM, Mays DJ, Pino MF, Tang LJ, Pietenpol JA. A gene signature-based approach identifies mTOR as a regulator of p73. Mol Cell Biol. 2008;28(19):5951-64.
97. Kato H, Nakajima S, Saito Y, Takahashi S, Katoh R, Kitamura M. mTORC1 serves ER stress-triggered apoptosis via selective activation of the IRE1-JNK pathway. Cell Death Differ. 2012;19(2):310-20.
98. Hsu PP, Kang SA, Rameseder J, Zhang Y, Ottina KA, Lim D, Peterson TR, Choi Y, Gray NS, Yaffe MB, Marto JA, Sabatini DM. The mTOR-regulated phosphoproteome reveals a mechanism of mTORC1-mediated inhibition of growth factor signaling. Science. 2011;332(6035):1317-22.
99. Scian MJ, Carchman EH, Mohanraj L, Stagliano KE, Anderson MA, Deb D, Crane BM, Kiyono T, Windle B, Deb SP, Deb S. Wild-type p53 and p73 negatively regulate expression of proliferation related genes. Oncogene. 2008;27(18):2583-93.
100. Honnappa S, Gouveia SM, Weisbrich A, Damberger FF, Bhavesh NS, Jawhari H, Grigoriev I, van Rijssel FJ, Buey RM, Lawera A, Jelesarov I, Winkler FK, Wüthrich K, Akhmanova

A, Steinmetz MO. An EB1-binding motif acts as a microtubule tip localization signal. Cell. 2009;138(2):366-76.

101. Malik R, et al. Quantitative analysis of the human spindle phosphoproteome at distinct mitotic stages. J Proteome Res 2009; 8: 4553-63.

102. Tsuji T, Ficarro SB, Jiang W. Essential role of phosphorylation of MCM2 by Cdc7/Dbf4 in the initiation of DNA replication in mammalian cells. Mol Biol Cell. 2006;17(10):4459-72.

103. Decuypere JP, Welkenhuyzen K, Luyten T, Ponsaerts R, Dewaele M, Molgó J, Agostinis P, Missiaen L, De Smedt H, Parys JB, Bultynck G. Ins(1,4,5)P3 receptor-mediated Ca2+ signaling and autophagy induction are interrelated. Autophagy. 2011;7(12):1472-89.

104. Ashrafi G, Schwarz TL. The pathways of mitophagy for quality control and clearance of mitochondria. Cell Death Differ. 2013 Jan;20(1):31-42.

105. Maiuri MC, Zalckvar E, Kimchi A, Kroemer G. Self-eating and self-killing: crosstalk between autophagy and apoptosis. Nat Rev Mol Cell Biol. 2007;8(9):741-52.

106. Hanamoto T, Ozaki T, Furuya K, Hosoda M, Hayashi S, Nakanishi M, Yamamoto H, Kikuchi H, Todo S, Nakagawara A. Identification of protein kinase A catalytic subunit beta as a novel binding partner of p73 and regulation of p73 function. J Biol Chem. 2005;280(17):16665-75.

107. D'Alessandro A, Zolla L. Metabolomics and cancer drug discovery: let the cells do the talking. Drug Discov Today. 2012;17(1-2):3-9.

108. Coates PJ, Nenutil R, McGregor A, Picksley SM, Crouch DH, Hall PA, Wright EG. Mammalian prohibitin proteins respond to mitochondrial stress and decrease during cellular senescence. Exp Cell Res. 2001;265(2):262-73.

109. Surovtseva YV, Shutt TE, Cotney J, Cimen H, Chen SY, Koc EC, Shadel GS. Mitochondrial ribosomal protein L12 selectively associates with human mitochondrial RNA polymerase to activate transcription. Proc Natl Acad Sci U S A. 2011;108(44):17921-6.

110. Cheong H, Lu C, Lindsten T, Thompson CB. Therapeutic targets in cancer cell metabolism and autophagy. Nat Biotechnol. 2012;30(7):671-8.

111. Sbisà E, Catalano D, Grillo G, et al. p53FamTaG: a database resource of human p53, p63 and p73 direct target genes combining in silico prediction and microarray data. BMC Bioinformatics 2007; 8 Suppl 1:S20.

112. Hu W, Zhang C, Wu R, Sun Y, Levine A, Feng Z. Glutaminase 2, a novel p53 target gene regulating energy metabolism and antioxidant function. Proc Natl Acad Sci U S A. 2010;107(16):7455-60.

113. Suzuki S, Tanaka T, Poyurovsky MV, Nagano H, Mayama T, Ohkubo S, Lokshin M, Hosokawa H, Nakayama T, Suzuki Y, Sugano S, Sato E, Nagao T, Yokote K, Tatsuno I, Prives C. Phosphate-activated glutaminase (GLS2), a p53-inducible regulator of glutamine metabolism and reactive oxygen species. Proc Natl Acad Sci U S A. 2010;107(16):7461-6.
114. Jiang P, Du W, Wang X, Mancuso A, Gao X, Wu M, Yang X. p53 regulates biosynthesis through direct inactivation of glucose-6-phosphate dehydrogenase. Nat Cell Biol. 2011 Mar;13(3):310-6.
115. Tullo A, Mastropasqua G, Bourdon JC, Centonze P, Gostissa M, Costanzo A, Levrero M, Del Sal G, Saccone C, Sbisà E. Adenosine deaminase, a key enzyme in DNA precursors control, is a new p73 target. Oncogene. 2003;22(54):8738-48.
116. Mori M. Regulation of nitric oxide synthesis and apoptosis by arginase and arginine recycling. J Nutr. 2007;137(6-2):1616S-1620S.
117. D'Erchia AM, Tullo A, Lefkimmiatis K, Saccone C, Sbisà E. The fatty acid synthase gene is a conserved p53 family target from worm to human. Cell Cycle 2006;5:750–8.
118. Ford JH. Saturated fatty acid metabolism is key link between cell division, cancer, and senescence in cellular and whole organism aging. Age (Dordr). 2010;32(2):231-7.
119. Liberles SD, Schreiber SL. Apoptosis-inducing natural products found in utero during murine pregnancy. Chem Biol. 2000;7(5):365-72.
120. Pettus BJ, Chalfant CE, Hannun YA. Ceramide in apoptosis: an overview and current perspectives. Biochim Biophys Acta. 2002;1585(2-3):114-25.
121. Bourbon NA, Sandirasegarane L, Kester M. Ceramide-induced inhibition of Akt is mediated through protein kinase Czeta: implications for growth arrest. J Biol Chem. 2002;277(5):3286-92.
122. Stoica BA, Movsesyan VA, Lea PM 4th, Faden AI. Ceramide-induced neuronal apoptosis is associated with dephosphorylation of Akt, BAD, FKHR, GSK-3beta, and induction of the mitochondrial-dependent intrinsic caspase pathway. Mol Cell Neurosci. 2003;22(3):365-82.
123. Das UN. Essential fatty acids, lipid peroxidation and apoptosis. Prostaglandins Leukot Essent Fatty Acids. 1999;61(3):157-63.
124. González-Santamaría J, Campagna M, Ortega-Molina A, Marcos-Villar L, de la Cruz-Herrera CF, González D, Gallego P, Lopitz-Otsoa F, Esteban M, Rodríguez MS, Serrano M, Rivas C. Regulation of the tumor suppressor PTEN by SUMO. Cell Death Dis. 2012;3:e393

125. Luo H, Yang Y, Duan J, Wu P, Jiang Q, Xu C. PTEN-regulated AKT/FoxO3a/Bim signaling contributes to reactive oxygen species-mediated apoptosis in selenite-treated colorectal cancer cells. Cell Death Dis. 2013;4:e481